NAVAL POSTGRADUATE SCHOOL

MONTEREY, CALIFORNIA

THESIS

METEOROLOGICAL MEASUREMENTS WITH A MWR-05XP PHASED ARRAY RADAR

by

John B. Sandifer

March 2005

Thesis Advisor:	Jeffrey B. Knorr
Thesis Co-Advisor:	Carlyle H. Wash

Approved for public release; distribution is unlimited.

THIS PAGE INTENTIONALLY LEFT BLANK

REPORT DOCUMENTATION PAGE			*Form Approved OMB No. 0704-0188*
Public reporting burden for this collection of information is estimated to average 1 hour per response, including the time for reviewing instruction, searching existing data sources, gathering and maintaining the data needed, and completing and reviewing the collection of information. Send comments regarding this burden estimate or any other aspect of this collection of information, including suggestions for reducing this burden, to Washington headquarters Services, Directorate for Information Operations and Reports, 1215 Jefferson Davis Highway, Suite 1204, Arlington, VA 22202-4302, and to the Office of Management and Budget, Paperwork Reduction Project (0704-0188) Washington DC 20503.			
1. AGENCY USE ONLY *(Leave blank)*	2. REPORT DATE March 2005	3. REPORT TYPE AND DATES COVERED Master's Thesis	
4. TITLE AND SUBTITLE: Meteorological Measurements with a MWR-05XP Phased Array Radar			5. FUNDING NUMBERS
6. AUTHOR(S) John B. Sandifer			
7. PERFORMING ORGANIZATION NAME(S) AND ADDRESS(ES) Naval Postgraduate School Monterey, CA 93943-5000			8. PERFORMING ORGANIZATION REPORT NUMBER
9. SPONSORING /MONITORING AGENCY NAME(S) AND ADDRESS(ES) N/A			10. SPONSORING/MONITORING AGENCY REPORT NUMBER
11. SUPPLEMENTARY NOTES The views expressed in this thesis are those of the author and do not reflect the official policy or position of the Department of Defense or the U.S. Government.			
12a. DISTRIBUTION / AVAILABILITY STATEMENT Approved for public release; distribution is unlimited.			12b. DISTRIBUTION CODE

13. ABSTRACT (maximum 200 words)

Scanning strategies for research and operational applications were developed for meteorological measurements with an experimental PAR, the MWR-05XP. A tornadic storm sampling strategy was developed with a 502.26 ms volumetric update and a resolution of 1.8° Az x 2° El x 150 m range. A sampling strategy for severe thunderstorm clusters was developed with a 10 second volumetric update and a resolution of 1.8° Az x 2° El x 300 m range. An operational weather scanning strategy was developed with an 81 second volumetric update and a resolution of 1.8° Az x 2° El x 150 m range. In general, for the acquisition of weather data, single frequency phased array radars offer only a slight sampling advantage over conventional scanning radars. This research verified that for meteorological sampling with the MWR-05XP, frequency diversity, coupled with electronic elevation scanning, offers a significant sampling advantage over conventional radars. The combination of electronic beam steering and frequency diversity produces a synergistic reduction in sampling time that increases the overall volumetric update rate. This research has also shown that, based on assumptions about the MWR-05XP operating parameters, it is possible to incorporate operational weather scanning into the radar's multifunction capability.

14. SUBJECT TERMS Phased Array Radar, Beam Steering, Frequency Steering, Meteorological Scanning, Weather Radar, Sampling Strategy, Scanning Strategy, Weather Scanning, MWR-05XP, Doppler Spectrum, Reflectivity, Doppler Velocity, Spectrum Width, Meteorological Moment Estimators, Tornado Radar Measurements, Tornado Chasing, Storm Chasing.	15. NUMBER OF PAGES 97
	16. PRICE CODE

17. SECURITY CLASSIFICATION OF REPORT	18. SECURITY CLASSIFICATION OF THIS PAGE	19. SECURITY CLASSIFICATION OF ABSTRACT	20. LIMITATION OF ABSTRACT
Unclassified	Unclassified	Unclassified	UL

NSN 7540-01-280-5500

Standard Form 298 (Rev. 2-89)
Prescribed by ANSI Std. 239-18

THIS PAGE INTENTIONALLY LEFT BLANK

Approved for public release; distribution is unlimited.

METEOROLOGICAL MEASUREMENTS WITH A MWR-05XP PHASED ARRAY RADAR

John B. Sandifer
Captain, United States Air Force
B.S., University of Arizona, 1998

Submitted in partial fulfillment of the
requirements for the degree of

MASTER OF SCIENCE IN METEOROLOGY

from the

NAVAL POSTGRADUATE SCHOOL
March 2005

Author: John B. Sandifer

Approved by: Jeffrey B. Knorr
Thesis Advisor

Carlyle H. Wash
Thesis Co-Advisor

Philip A. Durkee
Chairman, Department of Meteorology

THIS PAGE INTENTIONALLY LEFT BLANK

ABSTRACT

Scanning strategies for research and operational applications were developed for meteorological measurements with an experimental phased array radar, the MWR-05XP. A tornadic storm sampling strategy was developed with a 502.26 ms volumetric update and a resolution of 1.8° Az x 2° El x 150 m range. A sampling strategy for severe thunderstorm clusters was developed with a 10 second volumetric update and a resolution of 1.8° Az x 2° El x 300 m range. An operational weather scanning strategy was developed with an 81 second volumetric update and a resolution of 1.8° Az x 2° El x 150 m range. In general, for the acquisition of weather data, single frequency phased array radars offer only a slight sampling advantage over conventional scanning radars. This research verified that for meteorological sampling with the MWR-05XP, frequency diversity, coupled with electronic elevation scanning, offers a significant sampling advantage over conventional radars. The combination of electronic beam steering and frequency diversity produces a synergistic reduction in sampling time that increases the overall volumetric update rate. This research has also shown that, based on assumptions about the MWR-05XP operating parameters, it is possible to incorporate operational weather scanning into the radar's multifunction capability.

THIS PAGE INTENTIONALLY LEFT BLANK

TABLE OF CONTENTS

I. INTRODUCTION 1
A. BACKGROUND 1
B. THESIS OBJECTIVE AND SCOPE 2
C. THESIS APPROACH 3
D. RELATED WORK 3
1. Phased Array Radar 3
2. Doppler Radar Wind Spectra 4

II. PHASED ARRAY WEATHER RADAR 7
A. RADAR SYSTEM CONCEPT 7
B. PHASED ARRAY ANTENNA PRINCIPLES 9
C. MWR-05XP OVERVIEW 11

III. MATHEMATICAL DEVELOPMENT FOR METEOROLOGICAL MEASUREMENTS 21
A. BASIC RADAR EQUATIONS 21
1. Fundamental Relationships 21
2. Power Received 24
3. Noise and Integration 25
4. Power Received from Meteorological Targets 27
B. SPECTRAL MOMENTS 29
1. Introduction 29
2. Gaussian Distribution of Meteorological Targets 30
3. The Doppler Spectrum 32
4. Meteorological Moment Estimators 35
5. Correlation and Coherency 38

IV. PROPOSED SCANNING STRATEGIES FOR RESEARCH APPLICATIONS 43
A. RELATING SPECTRUM WIDTH DATA TO VARIOUS WEATHER CONDITIONS 43
1. WSR-88D Spectrum Width Error Sources 44
2. Censoring Erroneous WSR-88D Spectrum Width Data 44
B. SPATIAL AND TEMPORAL SAMPLING SCALES 45
1. Isolated Supercell Tornadic Storms 45
2. Multicellular Severe Storm Clusters 47
C. ACCURACY OF MOMENT ESTIMATES 48
D. DEVELOPMENT OF SAMPLING SCHEMES 50
1. General Considerations 50
2. Isolated Tornadic Storms 52
3. Multicellular Severe Storm Clusters 53

V. PROPOSED SCANNING STRATEGY FOR OPERATIONAL APPLICATIONS 57
A. ASSUMPTIONS AND COMPROMISES FOR OPERATIONAL WEATHER SCANNING 57
B. SAMPLING SCHEME FOR OPERATIONAL WEATHER SCANNING 59
C. ACCURACY OF MOMENT ESTIMATES 63
VI. CONCLUSIONS AND RECOMMENDATIONS 65
A. CONCLUSIONS 65
B. RECOMMENDATIONS FOR CONTINUED DEVELOPMENT 67
1. Calibration 67
2. Pointing Correction Algorithm 69
3. Verification of Velocity and Range Dealiasing Algorithms. 69
4. Modification for 1 MHz Frequency Scanning Increments. 70
5. Develop a Standard Suite of Output Products. 70
6. Strategies for Improved Spectrum Width Measurements. 71
7. Strategies to Minimize Ground Clutter. 71
8. Operational Meteorological Scanning Strategies 72
9. Integrate OMD into COP for Battlefield Commanders. 72
C. RECOMMENDATIONS FOR FUTURE STUDIES 72
1. Severe Storm and Tornado Measurements in Central US 72
2. Waterspout Measurements on Florida Coast 73
3. Stratiform and Convective Precipitation Measurements 73
LIST OF REFERENCES 75
INITIAL DISTRIBUTION LIST 79

LIST OF FIGURES

Figure 2.1. Simplified block diagram of a Doppler radar. 8
Figure 2.2. Linear five element phased array. 10
Figure 2.3. AN/MPQ-64 PAR (From PopStefanija et al. 2003). 12
Figure 2.4. MWR-05XP system block diagram (After PopStefanija et al. 2003). 13
Figure 2.5. MWR-05XP truck driving configuration (After Knorr 4 Feb, 2005). 13
Figure 2.6. MWR-05XP truck operating configuration (After Knorr 4 Feb, 2005). 14
Figure 2.7. MWR-05XP System (From Knorr 16 Mar, 2005). 14
Figure 2.8. Single-pulse precipitation performance (From Knorr 31 Jan, 2005). 16
Figure 2.9. Single-pulse clear air performance (From Knorr 31 Jan, 2005). 16
Figure 2.10. WRP block diagram (From PopStefanija 2005). 17
Figure 2.11. MWR-05XP GUI display (After PopStefanija 15 Oct, 2004). 19
Figure 2.12. MWR-05XP scanning modes (After PopStefanija 15 Oct, 2004). 19
Figure 3.1. Travel time of the radar pulse (After Knorr and Jenn 2004). 22
Figure 3.2. Pulse radar transmission (After Knorr and Jenn 2004). 22
Figure 3.3. Peak and average power (After Knorr and Jenn 2004). 27
Figure 3.4. Fluctuating power of the received echo (From Sauvageot 1992). 30
Figure 3.5. Probability distribution of the mean of k independent values of the signal power when average power is $\overline{P}$ (From Marshall and Hitschfeld 1953). 31
Figure 3.6. Estimation of $\overline{P}$ as a function of the number of independent pulses used to calculate the average (From Marshall and Hitschfeld 1953). 32
Figure 3.7. The Doppler spectrum (Figure a From Sauvageot 1992, Figure b From Skolnik 1990). 34
Figure 3.8. Independent sampling time versus spectrum width (From Sauvageot 1992). 40
Figure 3.9. Spectrum width versus max unambiguous range for correlated samples (After Doviak and Zrnic 1993). 41
Figure 4.1. Radar electronic elevation scan for tornado measurements. 46
Figure 4.2. Radar azimuth frequency scan for tornado measurements. 46
Figure 4.3. Radar electronic elevation scan for multicellular storms. 47
Figure 4.4. Radar 45° mechanical arc scan for multicellular storms. 48
Figure 4.5. MWR-05XP beam steering (After PopStefanija 28 Oct, 2004). 52
Figure 4.6. Proposed tornado Doppler sampling strategy. 53
Figure 4.7. Proposed severe storm cluster Doppler sampling strategy. 56
Figure 5.1. MWR-05XP operational radar scan geometry. 58
Figure 5.2. MWR-05XP operational weather scan coverage. 59
Figure 5.3. Proposed operational weather scan sampling strategy (lower elevation). 61
Figure 5.4. Proposed operational weather scan sampling strategy (upper elevation). 62
Figure 6.1. MWR-05XP preliminary receiver calibration. 68
Figure 6.2. GPS indicated beam pointing versus actual beam pointing. 69

THIS PAGE INTENTIONALLY LEFT BLANK

LIST OF TABLES

Table 2.1. MWR-05XP key system parameters.....15
Table 6.1. WSR-88D products and algorithms for possible application as MWR-05XP output products. 71

THIS PAGE INTENTIONALLY LEFT BLANK

LIST OF ACRONYMS AND ABBREVIATIONS

ATG	Antenna Group
AGC	Automatic Gain Control
AZ	Azimuth
CIRPAS	Center For Interdisciplinary Remotely Piloted Aircraft Studies
COP	Common Operating Picture
COHO	Coherent Oscillator
DOW	Doppler On Wheels
EL	Elevation
FPGA	Field Programmable Gated Array
GPS	Global Positioning System
GUI	Graphical User Interface
IF	Intermediate Frequency
MWR-05XP	Mobile Weather Radar, 2005, X-Band, Phased Array
NCAR	National Center For Atmospheric Research
NEXRAD	Next Generation Radar WSR-88D
NPS	Naval Post Graduate School
NSSL	National Severe Storms Laboratory
NWRT	National Weather Radar Testbed
OMD	Operational Meteorological Data
PAR	Phased Array Radar
PIN	Positive Intrinsic Negative

PPI	Plan Position Indicator
PRF	Pulse Repetition Frequency
PRT	Pulse Repetition Time
RF	Radio Frequency
RHI	Range Height Indicator
RPM	Revolutions Per Minute
RRE	Radar Range Equation
RX	Receiver
SNR	Signal To Noise Ratio
STALO	Stable Local Oscillator
SW	Spectrum Width
TWR	Tactical Weather Radar
WRP	Weather Radar Processor
WSR-88D	Weather Surveillance Radar, 1988, Doppler

ACKNOWLEDGMENTS

A project of this magnitude, working with an untested and, during the time of this thesis, unavailable radar, provided many opportunities for frustration and failure. I chose to stick it out because I believe this radar technology is a meteorological "diamond in the rough", and will eventually save lives. I hope my humble, simple efforts will inspire others, much smarter than myself, to think outside the box.

I want to express my gratitude to my advisors, Prof. Jeff Knorr and Prof. Chuck Wash for their guidance, mentoring, and willingness to work across disciplines to provide me this opportunity. Prof. Knorr is one of the smartest men I know and I appreciate the time he took to explain and re-explain the fundamentals to me. Prof Wash kept me focused, and provided invaluable insight to maintain an operational perspective. I also want to thank Prof. "Haf" Jonsson, whose excitement, both about flying an underpowered plane in zero visibility and about this radar, initially sparked my interest in the project, and whose definition of serendipity I will never forget. I also want to thank my Air Force buddies, Captains Jeff Jarry and Clay Baskin. We were collectively known as the leper colony yet we made it. Proof yet again that if I can do it, anyone can. Thank you gentlemen, it has been a pleasure working with you and keeping the Air Force NPS flag flying high.

Finally, I would like to thank God and my family for their prayers and support. To my loving and patient wife, Katrina, and my son, Corey, thank you for your support and understanding during the many ups and downs of this project. I wouldn't be here today if it weren't for you. It is indeed an honor and privilege to serve this great nation and you are the reason I choose to do so. I trust that others will continue to serve with me in a myriad of ways, be it building a bridge, painting a picture, or simply being kind to a neighbor.

THIS PAGE INTENTIONALLY LEFT BLANK

I. INTRODUCTION

A. BACKGROUND

As technologies expand and technological prowess grows so has the realization that along with these advances vulnerabilities also grow. Technology forces users to favor fewer, more capable systems that tend to cluster in strategic centers of operation as system complexity, capabilities, and costs rise. Consequently, the potential for loss or damage is increased when these centers of material and personnel are impacted by meso and microscale weather events. Tactical weather radars (TWR) are key to protecting these operation centers from the only enemy for which there is no defense, the weather. Without these radars to provide advance warning of damaging weather, users are unable to take appropriate protective measures to prevent loss of resources, readiness, and even lives. In addition, TWRs can provide detailed real-time information to war-fighters allowing them to exploit the weather to our advantage and to our enemies' disadvantage.

Currently, there are no TWRs designed for use in high threat forward operating areas. The few fielded systems are primarily designed for use behind friendly lines in air asset support roles at airports and temporary landing strips. Mobile Phased Array Radars (PAR) are an integral part of our offensive and defensive weapons systems and are routinely used in forward operating areas to detect and track multiple targets. Many of these tactical radars are also suitable, in terms of transmitting power and operating frequency, for use in making basic meteorological measurements. Therefore, the concept of adding a weather processor to these radars should be considered. In theory, Weather Radar Processors (WRP) can be cost effectively added to existing tactical PARs to provide critical weather intelligence without compromising battlefield awareness.

One suitable tactical radar is the AN/MPQ-64 mobile Forward Area Air Defense radar currently used by the US Army. The Navy Center for Interdisciplinary Remotely Piloted Aircraft Studies (CIRPAS) is collaborating with ProSensing Inc. to add a weather surveillance mode to this rapid scanning PAR for research and possible military applications (PopStefanija et al 2003). The weather surveillance measurements are made with an add-on WRP developed for this and similar radars. The system has been re-

designated the MWR-05XP, Mobile Weather Radar, 2005, X-band, Phased Array. When delivered, this system will be the only mobile phased array Doppler weather radar in existence with multidimensional beam steering capability. It will provide researchers with high resolution temporal and spatial measurements of mesoscale weather events and also function as the testbed for future study to determine the benefit of radar data for tactical military applications. In order to determine feasibility for military applications, research of system capabilities, both theoretical and empirical, must be conducted. This thesis makes an attempt to address these first research steps.

B. THESIS OBJECTIVE AND SCOPE

In this thesis, scanning strategies for research and operational applications are developed for meteorological measurements with an experimental PAR, the MWR-05XP. The first objective of this research is to determine the temporal and spatial sampling strategies for specified weather phenomena. In particular, sampling strategies that take advantage of the fast scanning capability of a phased array radar are investigated. The second objective of this research is to determine how sampling strategy affects the quality of the estimates of the Doppler moments of the weather signal. These estimates are: 1) the reflectivity or zero moment estimate of the Doppler spectrum, 2) the mean Doppler velocity or first moment of the Doppler spectrum, and 3) the spectrum width or square root of the second moment of the Doppler spectrum. Based on these moment estimates and the MWR-05XP capabilities, scanning strategies for various weather phenomena will be proposed that take advantage of PAR fast scanning capability.

The scope of this thesis is confined to meteorological research and limited operational applications with the MWR-05XP. Much more work is required to determine its feasibility for operational military use as a weather radar. This thesis focuses on one research aspect, determining the first three spectral moments and developing appropriate sampling strategies for meteorological research and operational weather scanning. This work, along with other contributions, will provide the basis for further research with the MWR-05XP. With some of the groundwork thus laid for research applications, incorporation of the add-on WRP to operational AN/MPQ-64 radars for meteorological measurements may follow and should be addressed in future work.

C. THESIS APPROACH

A general overview of radar concepts and beam steering with phased array antennas is presented. This is followed by a more technical overview of the MWR-05XP and its add-on Weather Radar Processor (WRP). A mathematical development of the equations used to derive the spectral moment estimates follows.

The scanning strategies for proposed research and operational applications are then presented. For research, these strategies are derived by: 1) determining the scale, expected range of Doppler velocities, and spectrum widths for various weather phenomena, 2) determining the desired accuracy of the meteorological parameters, and 3) developing sampling requirements based on these values and the operational constraints of the MWR-05XP. For operational applications, the sampling strategy is determined by: 1) assumptions about the MWR-05XP operating parameters, and 2) compromises in accuracy and coverage to insure timely meteorological updates with minimum impact to normal radar functions. Proposed sampling schemes are presented based on these parameters. Finally, conclusions and recommendations for continued development and future studies are outlined.

D. RELATED WORK

1. Phased Array Radar

Forsyth (2003) at the National Severe Storms Laboratory (NSSL) provides an overview of the establishment of the National Weather Radar Testbed (NWRT) in Norman, Ok. The NWRT is adapting a AN/SPY-1 Navy phased array radar for weather measurements to determine if phased array technology will become the next significant technology advancement to improve the nation's weather services. The project is expected to take 10 to 15 years at an initial cost of $25 million. Using multiple beams and frequencies, PAR reduces the weather scan time to one minute from six minutes for the currently fielded WSR-88D. In addition to faster updates, the system will scan the atmosphere with more detail at lower elevations and re-scan areas of severe weather very quickly potentially increasing forecast warning lead times. PAR will gather storm information not currently available, such as rapid changes in the wind fields, to provide researchers a more thorough understanding of storm evolution.

Wurman and Randall (2004) discuss the development of a rapid-scanning Doppler on Wheels (Rapid-DOW) radar. They state the need for a mobile, rapid scanning radar based on radar data from tornadoes and hurricanes citing that: a) phenomena associated with tornado genesis evolve on timescales currently unobservable with conventional scanning radars, and b) wind streaks in the hurricane boundary layer evolve and translate quickly requiring observations at least every 10 seconds. The DOW radars used since 1995 to study atmospheric phenomena typically require 40 to 60 seconds for complete volumetric sector scans. The new Rapid DOW radar uses a phased array antenna to simultaneously transmit up to 10-frequency independent pencil beams in elevation with fast mechanical azimuthal scanning. The system will frequency-split the returned energy for parallel processing and produce partial volumetric data on the order of 10 seconds.

Doviak et al. (2001) outlines benefits and challenges of phased array weather radar. They discuss improved scanning times based upon agile beam scanning and large spectral bandwidths. They compute the increase in scanning rate over conventional radar by equating the variances of the estimates for reflectivity and velocity. Potential advantages of PAR are: a) faster update rates, b) improved angular resolution, c) better measurement of spectral moments in the presence of beam blockage, d) mitigation of ground clutter effects, e) simultaneous observation of weather and tracking of objects such as aircraft or balloons, and f) improved spectrum width measurements. Specific challenges of the technology include: a) a dual polarization phased array is needed to make a significant improvement in quantitative precipitation measurements, b) instantaneous retrieval of transverse winds may be possible by correlating signals received simultaneously on different portions of the phased array, c) clutter canceling in the beam switching mode requires special processing techniques that need to be validated, and d) scanning strategies that adaptively adjust the beam direction to the location of weather phenomena need to be developed.

2. Doppler Radar Wind Spectra

Bluestein et al. (1993) using a portable 3-cm Doppler radar collected close-range data at and below cloud base from six supercell tornadoes in the southern plains during the springs of 1990 and 1991. Data collection and analysis techniques are described and wind spectra from six tornadoes are presented and discussed. Maximum Doppler wind

speeds of 55–105 m s^{-1} were found in five of the tornadoes, wind speeds as high as 120–125 m s^{-1} were found in a large tornado during an outbreak on 26 April 1991. The variation in the spectrum across the 26 April tornado is presented. Standard and mobile soundings and surface data, used to determine the "thermodynamic speed limit" indicate that it was usually exceed by 50-100%. A comparison of Doppler spectra with simulated spectra suggests that the maximum reflectivity in supercell tornadoes lies well outside the core.

Fang and Doviak (2001) relate WSR-88D spectrum width data to various weather conditions. They discuss WSR-88D spectrum width (SW) error sources and a method of censoring erroneous width data to obtain reliable data for analysis. Their preliminary study provides values of spectrum width for various weather phenomena. Error sources for SW include: a) overlaid weather signals resulting from relatively short pulse repetition frequencies, b) low signal-to-noise ratios due to receiver noise and incorrect estimates of noise power, and c) incorrect setup of the automatic gain control circuits causing clipping of the weather signals producing harmonics of the weather spectrum. In this study, erroneous data is censored by raising the overlaid multiple trip weather signals threshold up to 20 dB from 5 dB. If one of the trip signals is 20 dB or more stronger than the sum of the other trip signals, then the spectral moments of the stronger signal can be estimated without significant error (within the specifications of the WSR-88D). Algorithms have been developed to select data with a signal power at least 20 dB higher than the sum of competing out-of-trip signals. Derived SW values are: a) less than 2 m s^{-1} for isolated tornadoes, supercells, daytime clear air, stratiform rain, and snow, b) median values of 2.3 to 3.8 m s^{-1} for widespread rain showers and severe storm clusters, and c) large values of 4.5 to 5.8 m s^{-1} for embedded areal squall lines.

THIS PAGE INTENTIONALLY LEFT BLANK

II. PHASED ARRAY WEATHER RADAR

A. RADAR SYSTEM CONCEPT

Most objects reflect radio waves similar to the way they reflect light. Radar operates by radiating electromagnetic energy and detecting the energy returned from reflecting targets (Skolnik 1990). Radio or radio frequency (RF) energy incident on an object is either reflected, transmitted through, or absorbed by the target. The manner in which RF energy interacts with the target depends on the target properties and the position and orientation of the target to the incident radiation. For radar systems, one is primarily interested in the reflected energy, specifically the portion of reflected energy backscattered toward the receiving antenna. The received radar echo provides information about the target such as distance, speed, or composition. The range to the target is found from the time it takes for the RF energy to travel to the target and back. The location of the target is determined from the azimuth, elevation, and range from which the returned echo is received. For moving targets, the radar can determine the trajectory, and, the Doppler shift in frequency of the return echo provides information on target radial speed.

Although radars are highly specialized for their intended use, most share common basic components. The following discussion is intended to provide a layman's understanding of a basic radar system. A simple block diagram of a Doppler radar is shown Figure 2.1.

The transmitter develops and amplifies the signal to be radiated by the antenna. The waveform generator, as its name implies, develops the pulsed Doppler waveforms at low power. The waveforms are amplified to the kilowatt (kw) level in the power amplifier which is generally a klystron for Doppler weather radars. A klystron is a specialized vacuum tube that coherently amplifies a reference signal so its output can be precisely controlled in amplitude, frequency and phase. For Doppler radar, an extremely small Doppler induced frequency shift must be detected by comparing the received and transmitted frequencies. In order to achieve this required high transmission stability, a Stable Local Oscillator (STALO) generates a signal which is mixed with a stable

Coherent Oscillator (COHO) in the mixer. The mixed signal results in a transmitter output signal that has a stable frequency and phase for later comparison with the received echo.

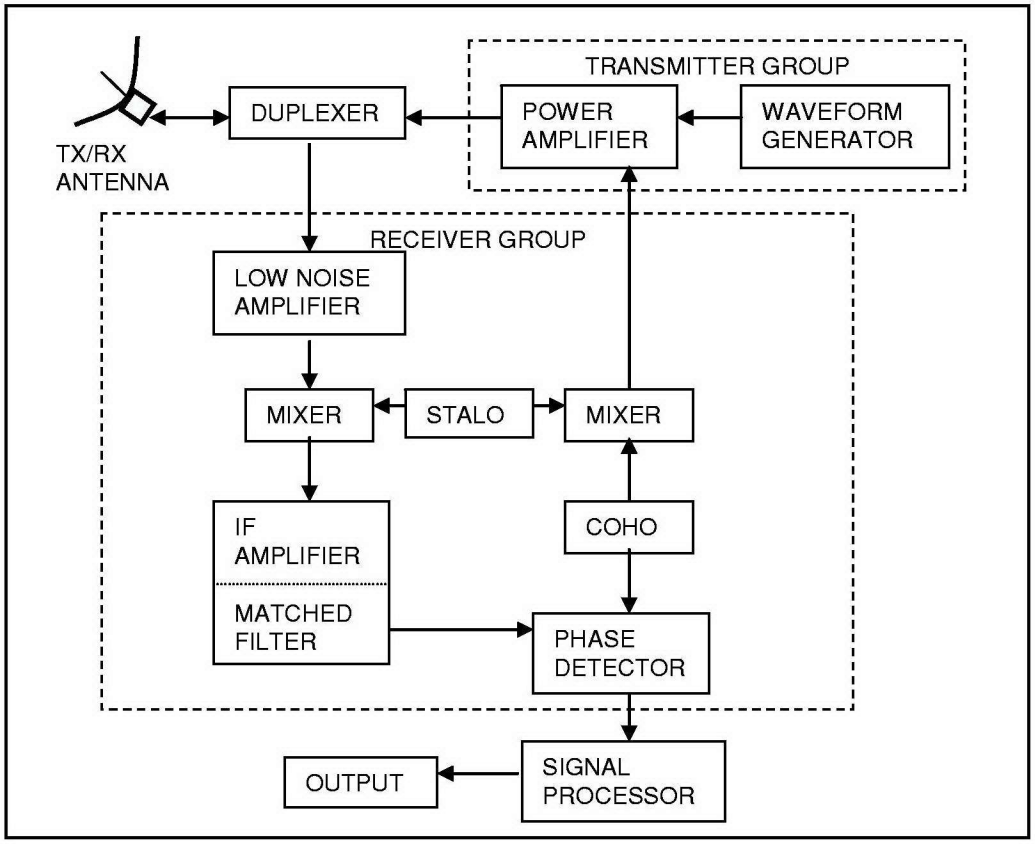

Figure 2.1. Simplified block diagram of a Doppler radar.

The duplexer, which is generally a gas-discharge device or solid state circulator, acts as a rapid single-pole-double-throw switch to connect the antenna to either the transmitter or receiver. The duplexer must completely isolate the sensitive receiver to prevent damage when the high power transmitter is on. After energy radiates from the antenna, the duplexer switches the transmitter off and connects the receiver to listen for return echoes. For most radars, the antenna both transmits high power RF and receives energy backscattered from atmospheric targets. This is known as a monostatic radar in which the transmitter and receiver are co-located and share a common antenna. The antenna radiates the transmitter power into space in a narrow beam. When the transmitter switches off, the antenna intercepts any backscattered energy and is connected to the receiver through the duplexer.

The return signal intercepted by the antenna is sent to the receiver. Doppler radar receivers are usually of the superheterodyne type. A superheterodyne receiver converts the received high frequency signal to a lower frequency for processing while preserving the phase information of the signal. The receiver separates the desired signal from other noise and signals and amplifies it for display or automated processing. In the receiver, the RF signal is converted down to an intermediate frequency (IF) in the mixer then amplified in the IF amplifier. A matched filter maximizes the signal-to-noise ratio (SNR) at the output of the IF amplifier to increase the detectability of the signal. The phase detector compares phase information of the received signal through the STALO to the phase of transmitted signal through the COHO. This phase difference gives the Doppler shift of the received signal.

The signal is then sent to the signal processor where correction algorithms such as velocity and range ambiguities are accomplished before further processing. Signal processing is not a distinct function as depicted in the block diagram however. Some functions of signal processing actually take place in the receiver in order to reject undesired signals and pass desired signals on to the detector. These functions include clutter rejection and Doppler filtering.

Processed data are passed to the output for display and/or storage. Some examples of output devices are video displays, audible warnings, printer outputs, or generation of other automated products. Weather radar data is often stored in analog or digital format for research, education, or training. More recently, output data has been used to assist in the initialization of storm scale and mesoscale weather models and also to provide real-time displays on the internet.

B. PHASED ARRAY ANTENNA PRINCIPLES

A phased array is a directive antenna made of smaller individual radiating antennas. It generates a radiation pattern whose shape and direction is determined by the relative phases and amplitudes of the individual antennas or elements. The radiating elements may consist of dipoles, open-ended waveguide, slots in waveguide, or printed-circuit patches. Phased arrays allow for fast and precise control of the radar beam. The

radar beam shape, direction, and even multiple beams can be generated with the phased array which adds tremendous utility to radar systems. This agile beam control permits faster scanning and allows the radar to perform multiple functions almost simultaneously such as scanning and multiple target tracking.

The phased array antenna shown in Figure 2.2 is a simple five element linear array. To steer the beam, power is applied to the radiating elements in a given order with a time delay between elements, rows, or groups of elements. This creates a phase difference across the array of radiators producing a composite wavefront due to constructive interference that can be electronically steered.

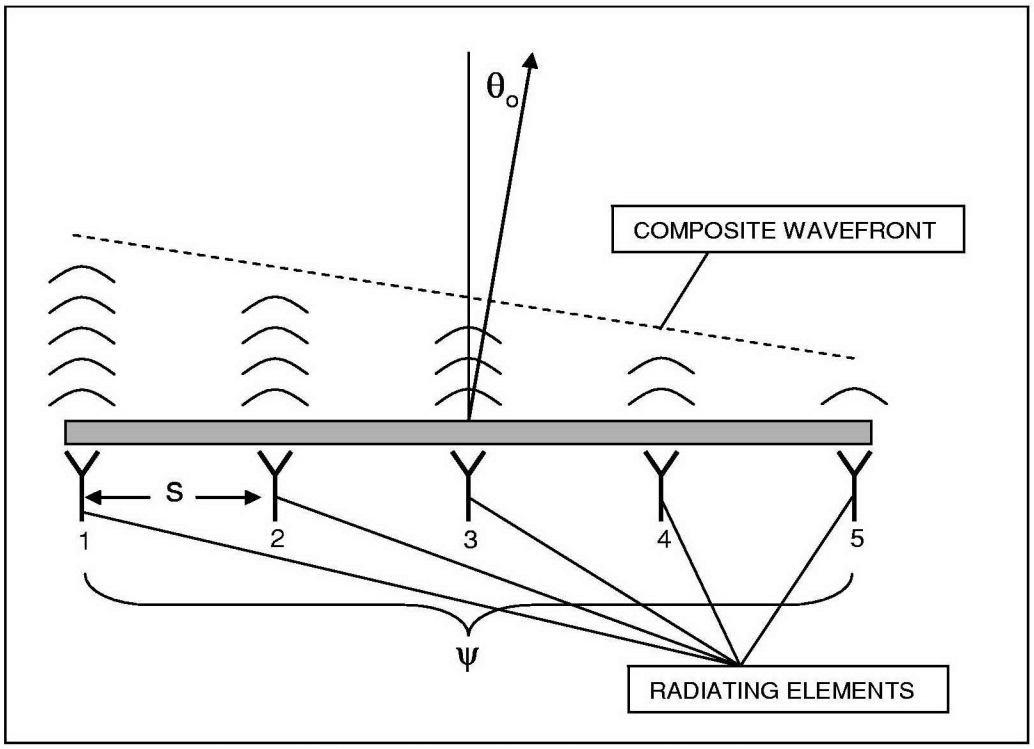

Figure 2.2. Linear five element phased array.

To steer the beam at an angle θ_o normal to the antenna face, a phase difference ψ is applied between adjacent elements, where ψ is given from Equation 2.1 (Skolnik 1990).

$$\Psi = \frac{2\pi s \sin(\theta_0)}{\lambda} \tag{2.1}$$

where: ψ = phase difference, in radians (rad), between two adjacent elements

s = distance, in meters (m), between two adjacent elements

λ = wavelength, in m, of transmitted signal

θ_o = angle, in degrees (°), of beam steering from normal

The basic techniques for electronic beam steering are frequency scanning and phase scanning with phase shifters. Frequency scanning is accomplished by slightly varying the transmitted frequency which changes the relative phase of the elements in the array resulting in beam steering. Phase scanning with phase shifters, discussed above, is the most popular approach. Both frequency and phase scanning are utilized with the radar in this thesis.

Beam steering with phase shifters is not a new technology. Early radar systems used antenna arrays because their lower operating frequencies required large antennas. As radar technology progressed into higher frequencies, most arrays were replaced by smaller, less expensive antennas such as the common parabolic reflector. In World War II, the United States, Great Britain, and Germany used large phased array antennas with mechanically actuated phase shifters to steer the beam. Crude electronic phase shifters replaced mechanical shifters by the early 1950s. Advances in electronics, computer aided design, and signal processing have fueled a renewed interest in phased array technology for research and military applications. Today, digitally switched phase shifters employing ferrites or Positive-Intrinsic-Negative (PIN) diodes allow beam steering in two dimensions.

C. MWR-05XP OVERVIEW

The key interest in PAR, or beam agile radar, for meteorological research is its extremely rapid scanning capability. According to Keeler and Frush (1983), the basic requirements for a rapid scanning meteorological radar is an ability to provide volume imaging of a large fraction of a hemisphere in less than 60 seconds with a beamwidth on the order of 1°. Other important requirements include a range resolution on the order of 200 m, operation at a frequency below 10 GHz to minimize attenuation, and sufficient sensitivity to track storms out to 50 km. One suitable tactical radar that meets these requirements is the AN/MPQ-64 Forward Area Air Defense radar currently used by the

US Army. It is a mobile, X-band, search and track radar with a phased array antenna combining electronic elevation and mechanical azimuth scanning (see Figure 2.3).

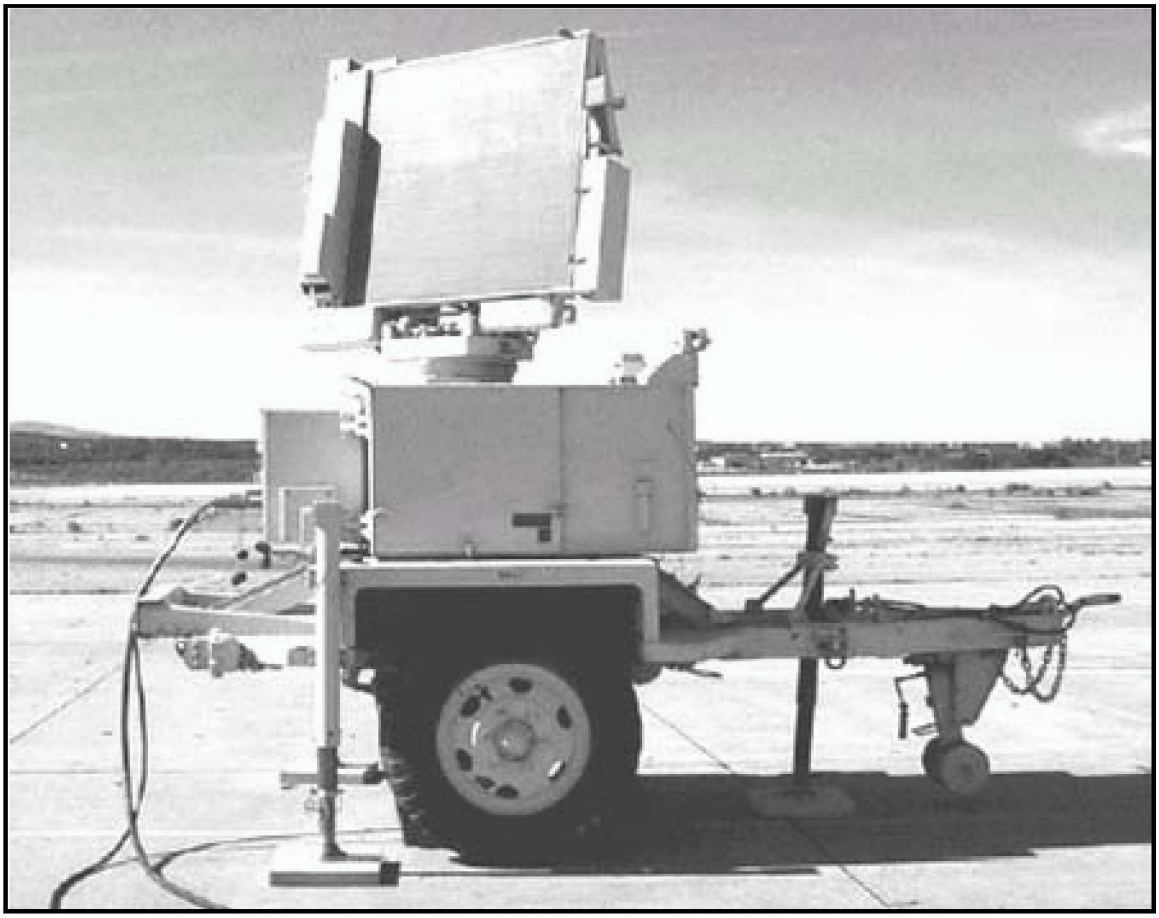

Figure 2.3. AN/MPQ-64 PAR (From PopStefanija et al. 2003).

The Naval Postgraduate School (NPS) Center for Interdisciplinary Remotely Piloted Aircraft Studies (CIRPAS) and the NPS Department of Electrical and Computer Engineering are collaborating with ProSensing Inc. to add a weather surveillance mode to this rapid scanning PAR for research and possible military applications (PopStefanija et al. 2003). The radar is jointly operated by CIRPAS and NPS in Monterey, CA. for education and research. ProSensing, based out of Amherst, MA., is developing an add-on Field Programmable Gated Array (FPGA)-based weather radar processor compatible with this and similar radars. The system will provide radar control, data acquisition, and signal processing for 3-D weather radar measurements. The system has been re-designated the MWR-05XP, Mobile Weather Radar, 2005, X-band, Phased Array. As part of the development effort, the system has been re-configured to fit all components

(antenna group (ATG), operator shelter, WRP) and a power generator on a flatbed truck (Figures 2.4 through 2.7) to improve system mobility and functionality for use as a mobile measurement laboratory similar to the Doppler on Wheels (DOW) research radars. When delivered, this system will be the only mobile phased array Doppler weather radar with multidimensional beam steering capability in existence. It will provide researchers with high resolution temporal and spatial measurements of mesoscale weather events and also function as the testbed for future study to determine the benefit of radar data for tactical military applications.

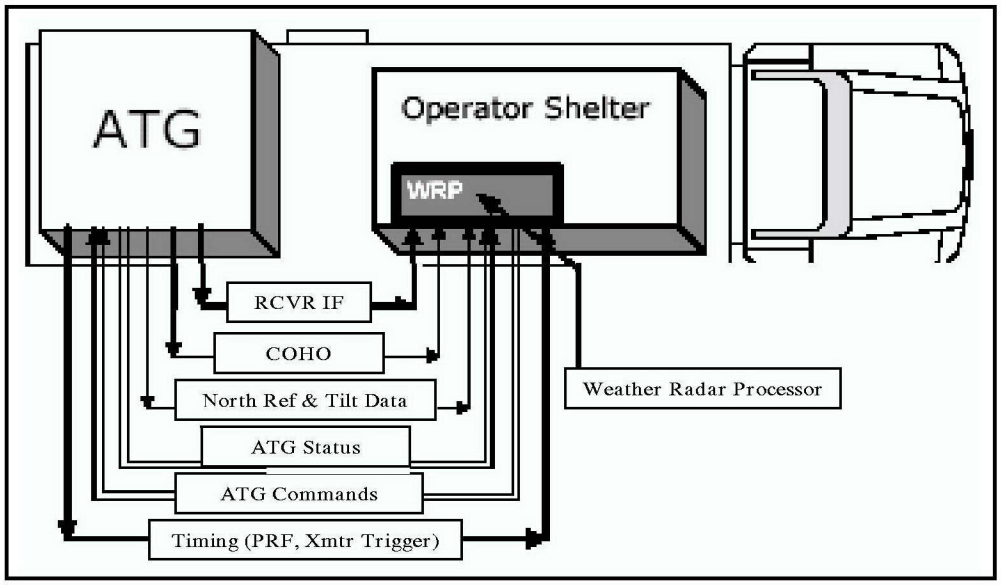

Figure 2.4. MWR-05XP system block diagram (After PopStefanija et al. 2003).

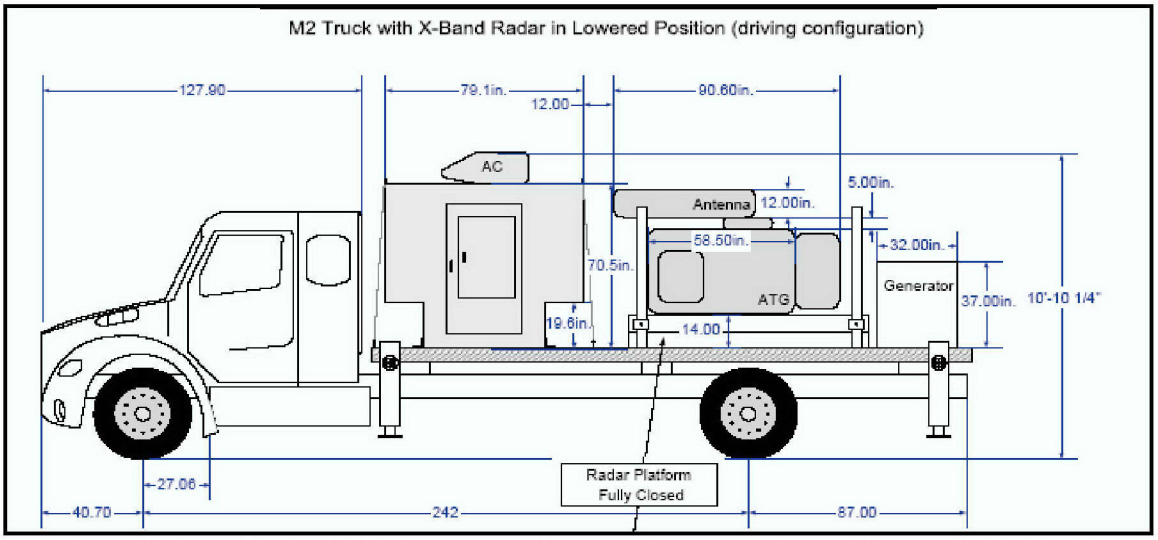

Figure 2.5. MWR-05XP truck driving configuration (After Knorr 4 Feb, 2005).

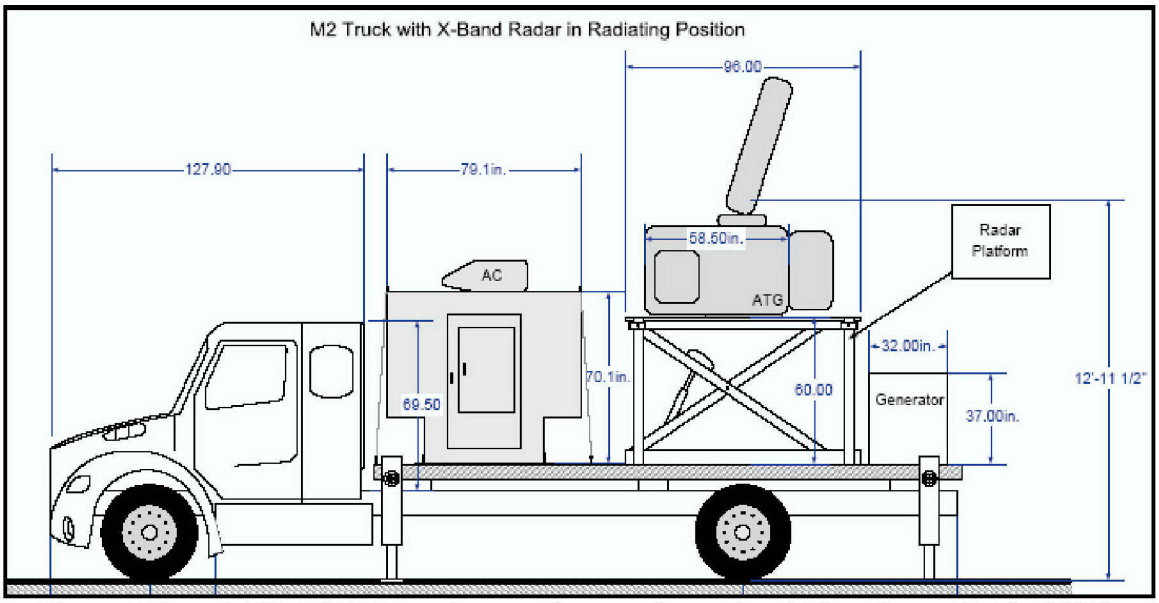

Figure 2.6. MWR-05XP truck operating configuration (After Knorr 4 Feb, 2005).

Figure 2.7. MWR-05XP System (From Knorr 16 Mar, 2005).

The radar beam can be mechanically scanned in azimuth (Az) over 360° at a rate of 3 or 30 rpm and electronically scanned in elevation (El) over a 22° sector. At 30 rpm, this 360°x22° volume can be uniformly sampled in only two seconds at a volumetric resolution of 1.8° Az x 2° El x 150 m range (PopStefanija et al. 2003). Antenna beam control and range resolution accuracy are 0.2° Az and El x 40 m range, which gives a volumetric pointing accuracy of 35m Az x 35m El x 40m range at 10 km. The antenna can also be frequency scanned in Az by +/- 3.5° allowing the beam to momentarily dwell on a fixed Az even while the antenna is rotating. The antenna also has an actuator arm which moves the antenna back and forth in a 45° arc. The fastest scanning rate with the actuator arm is 4 seconds per 45°. Other key radar parameters are listed in Table 2.1.

Certain parameters of the MWR-05XP are classified because an upgraded version of the radar is currently in use by the US Army. The values given are based on unclassified parameters and represent a lower resolution than actual system capabilities (Johnson 2000).

Transmitted Frequency	X-Band 9.37-9.99 GHz
Maximum Power	26 Kw
Operating Range	1 km to 75 km
PRF	488 Hz to 10 KHz
Receiver IF Frequency	96 MHz
Range Resolution	150 m (τ = 1 μ s)
System Floor Noise	-108 dB
Transmission Loss	4 dB
Antenna Aperture	1.2 m x 1.2 m
Beamwidth	1.8° Az x 2.0° El (pencil beam)
Scan Range	360° Az x -15° to +55° El

Table 2.1. MWR-05XP key system parameters.

From the radar range equation the expected single-pulse sensitivity vs. range performance of the MWR-05XP is plotted in Figures 2.8 and 2.9. Figure 2.8, for precipitation, shows how several values of radar reflectivity, *Z*, vary with range. The receiver noise, *RX Noise*, is approximately -108 dBm and represents the noise threshold below which single-pulse returns can not be distinguished from noise. Integrating pulses improves the SNR which increases sensitivity. The receiver saturation, *RX Sat*, is approximately -36 dBm and represents the level at which the receiver input is saturated. Clear air data, Figure 2.9, shows how several values of the refractive index vary with range. Clear air returns result from variations in the refractive index, C_n^2, due to turbulence. From the figure, it is clear that for detection, several pulses must be integrated to increase the SNR above the receiver noise threshold.

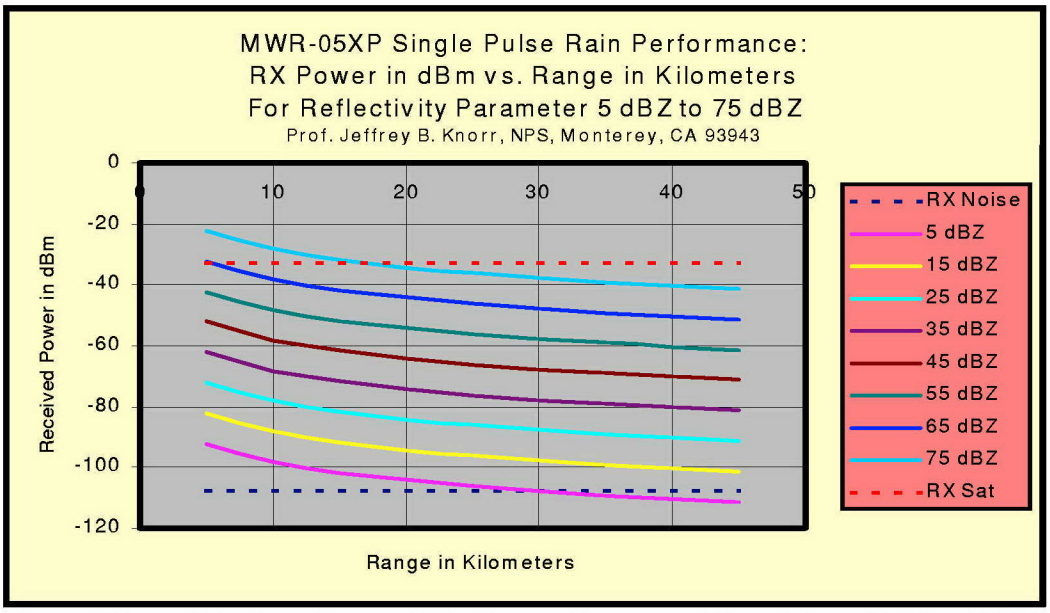

Figure 2.8. Single-pulse precipitation performance (From Knorr 31 Jan, 2005).

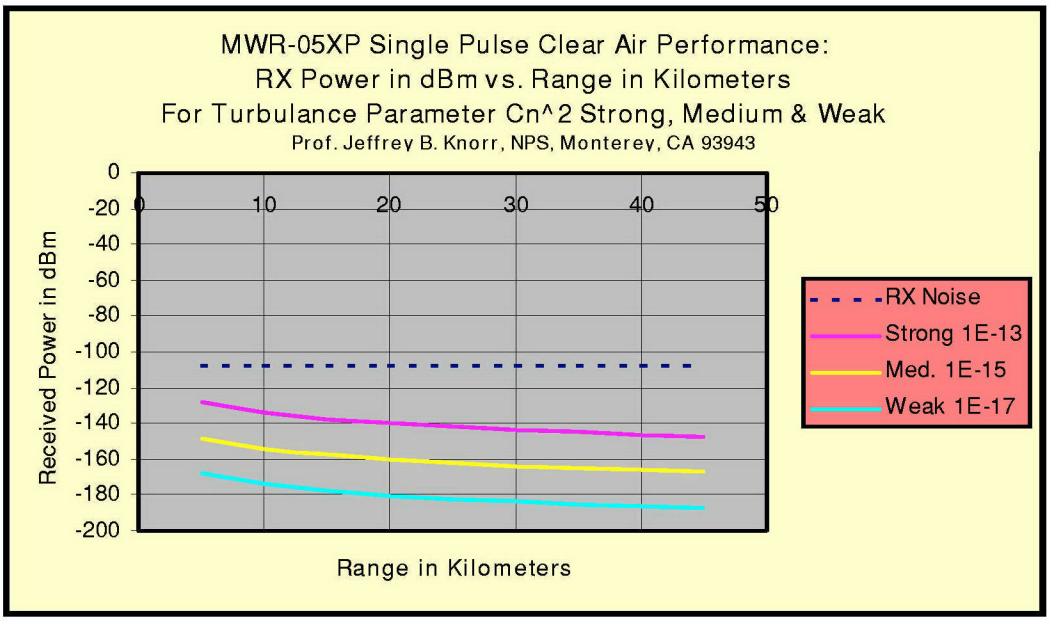

Figure 2.9. Single-pulse clear air performance (From Knorr 31 Jan, 2005).

The key element of the MWR-05XP for making meteorological measurements is the weather radar processor. The WRP system, block diagram shown in Figure 2.10, accepts IF signals from the radar and can either tie into existing control signals or can take control of the radar.

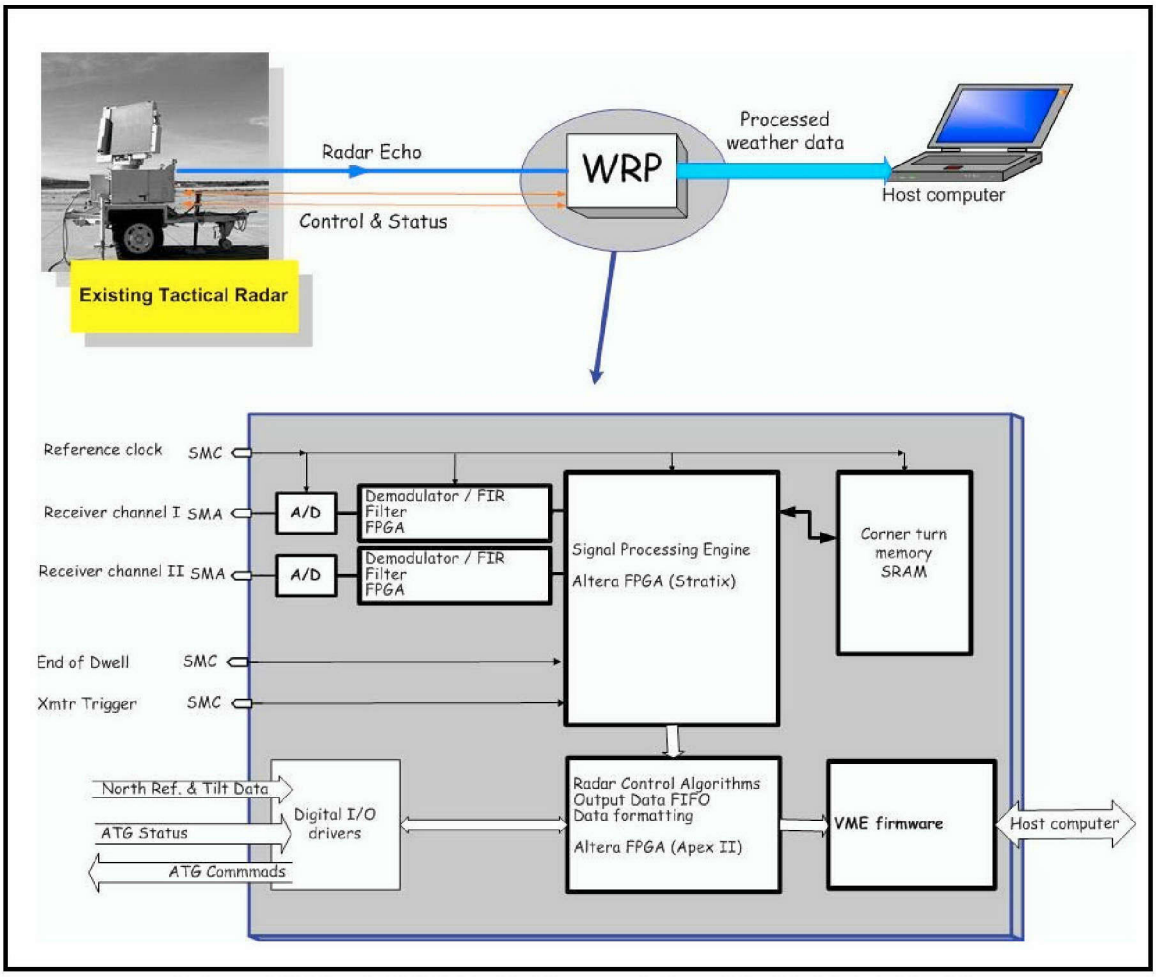

Figure 2.10. WRP block diagram (From PopStefanija 2005).

The WRP is controlled via a graphical user interface (GUI) which allows data display in a variety of formats. The WRP consists of two cards; a programmable FPGA-based controller, and a high performance digital receiver/signal processor. The FPGA controller, with its high performance processor, large external memory, and data averaging algorithms, offers superior computational speed with data throughput in excess of 1 Gbyte/s. The digital receiver/signal processor provides superior linearity and dynamic range over analog detection techniques. The WRP performs the following functions (Popstefanija et al. 2003):

1. All processing and data compression algorithms including notch filters for clutter rejection, staggered and dual pulse repetition time (PRT) for velocity dealiasing, digital I/Q detection, digital bandpass filtering, and pulse compression.

2. Radar control allowing instantaneous beam pointing angle control appropriate for weather surveillance.
3. Interface between radar and data system to merge raw radar data with auxiliary information such as antenna pointing angle, time, and GPS information.
4. Outputs reflectivity, pulse-pair derived velocity, and full-spectra at each sample volume in real time.
5. System control, post-processing, and display software.

The system currently provides real-time scrolling display of reflectivity and velocity. Reflectivity is currently a relative non-calibrated estimate. Spectral width, which is obtained from a Fast Fourier Transform algorithm, will be added for real-time display before final delivery in spring 2005. Data are also available in raw mode for post-processing. The software is adapted from ProSensing's processing and real-time display software already developed for previous weather radar applications. The meteorological moments (reflectivity, velocity, and spectrum width) will be displayed in real-time during data-gathering operations for on-line confirmation of data quality and integrity, and stored in universal radar format for post-processing by commercial software. Universal format includes raw radar reflectivity, velocity, and spectrum width data merged with auxiliary information such as antenna position, time, and GPS.

The radar GUI, shown in Figure 2.11, is displayed on a host laptop and is programmed with four scanning modes. These include (Popstefanija 2004):

1. Raster scan - user selectable start and stop points in both El and Az (see Figure 2.12a).
2. El scan - scans a vertical slice (fixed Az) with user selectable start and stop El points.
3. Fixed frequency El scan - same as El scan except the transmitted frequency is fixed which adds a slight arc to the scan (see Figure 2.12b).
4. Point - stares at a constant user selectable Az and El.

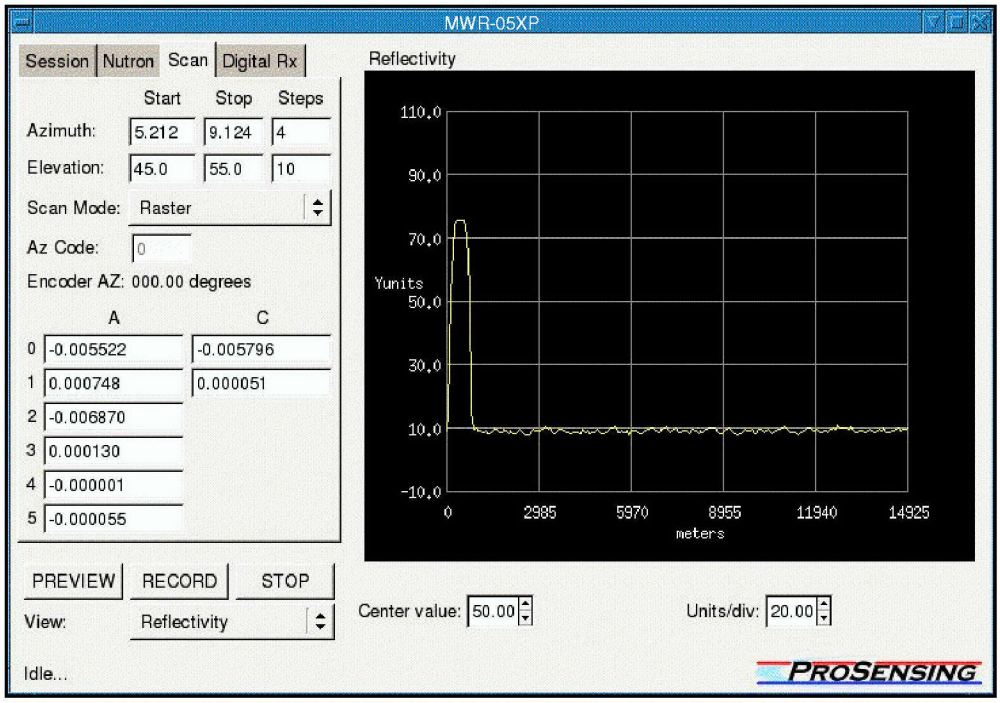

Figure 2.11. MWR-05XP GUI display (After PopStefanija 15 Oct, 2004).

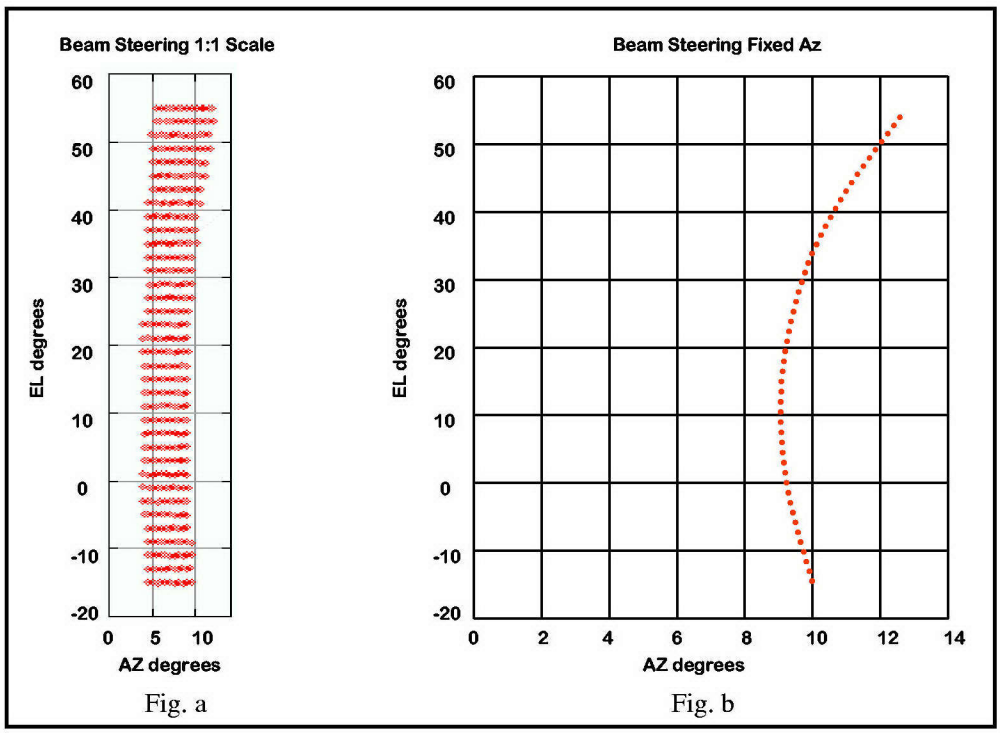

Fig. a Fig. b

Figure 2.12. MWR-05XP scanning modes (After PopStefanija 15 Oct, 2004).

THIS PAGE INTENTIONALLY LEFT BLANK

III. MATHEMATICAL DEVELOPMENT FOR METEOROLOGICAL MEASUREMENTS

A basic mathematical development of the equations used in this thesis is provided for interested readers. This chapter is intended only to provide a brief overview of the key equations and concepts for the purposes of attaining a basic conceptual understanding. For a more thorough treatment of radar theory, the reader is referred to advanced texts on the subject such as Raghaven 2003, Doviak and Zrnic 1993, Sauvageot 1992, or Skolnik 1990.

The main difference between weather radars and other types of radars lies in the nature of the targets to be detected. The atmosphere interacts significantly with both the transmitted and reflected energy, and, for many radar applications, produces undesirable weather clutter. This clutter is a result of absorption and reflection from numerous atmospheric constituents or phenomena such as: suspended industrial or natural particles, water vapor, precipitation, lightning, or strong thermal or humidity gradients. Other types of clutter include cosmic and man made noise. Many radar applications attempt to discriminate relatively few targets from this clutter background, for example, in the case of aircraft or missile tracking radars. Weather radars, however, focus on accurately estimating the parameters of the weather signal itself which provides radar designers with unique challenges. A familiarity with basic radar equations and a conceptual understanding of the weather signal Doppler power spectrum, correlation, and coherency are essential.

A. BASIC RADAR EQUATIONS

1. Fundamental Relationships

Range to a target is the most fundamental quantity typically measured by radars. The range is determined by measuring the round trip travel time, T_r, of a pulse from the radar to the target and back as shown in Figure 3.1. Following the development by Raghaven (2003), for a monostatic pulsed radar, the range, r, in meters is given by

$$r = \frac{ct}{2} \tag{3.1}$$

where c = speed of light in a vacuum, 3 x 10^8 m/s and t = time in seconds.

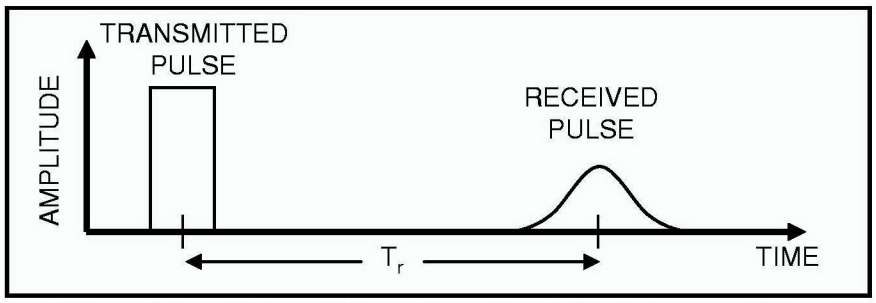

Figure 3.1. Travel time of the radar pulse (After Knorr and Jenn 2004).

In practice, a group of pulses, or pulse train, are transmitted in order to integrate several target returns to improve the chances of detection. Figure 3.2 shows a pulse train waveform where P_0 = pulse amplitude, τ = pulse width in seconds, and T_p = pulse period in seconds. If a target is moving with a radial component of velocity, v, both the range to

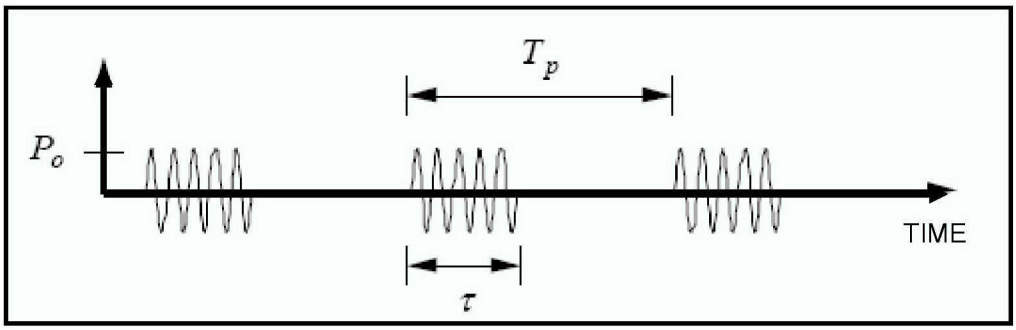

Figure 3.2. Pulse radar transmission (After Knorr and Jenn 2004).

the target, r, equation (3.1) and the phase shift, ϕ, change continuously. The phase shift, ϕ, is given by:

$$\phi = \frac{4\pi rf}{c} \tag{3.2}$$

where f = frequency of the radar. A change in ϕ with respect to time is a frequency. This is known as the Doppler angular frequency, ω, and is given as:

$$\omega = 2\pi F = \frac{d\phi}{dt} = \left[\frac{4\pi}{\lambda}\frac{dr}{dt}\right] = \frac{4\pi v}{\lambda} \tag{3.3}$$

where λ = wavelength of the radar, F = Doppler frequency shift, and v = radial component of velocity, or

$$F = \frac{2v}{r} = \frac{2vf}{c} \tag{3.4}$$

and

$$v = \frac{Fc}{2f} = \frac{F\lambda}{2}. \tag{3.5}$$

The number of pulses transmitted per second is called the pulse repetition frequency (PRF) and is the reciprocal of the time interval or period, T_p, between pulses. For example, a T_p of 1 millisecond equates to a PRF of 1 KHz. Applying a time of 1 millisecond to equation (3.1) gives a range of 150 km. This means the echoes from all targets within 150 km will arrive at the radar before the subsequent pulse is transmitted. Echoes from targets beyond 150 km will arrive after one or more subsequent pulses have been transmitted and are called multiple-trip echoes. These echoes will be displayed at an incorrect or ambiguous range which is equal to its true range minus a multiple of 150 km. The maximum unambiguous range, r_u, is:

$$r_u = \frac{c}{2(PRF)} \tag{3.6}$$

If the target is moving with a radial velocity component, its echo will be Doppler shifted as shown. The maximum Doppler shift, F_{max}, which can be detected without ambiguity is given by:

$$F_{\max} = \frac{PRF}{2} \tag{3.7}$$

Therefore, the maximum target velocity, v_u, which can be unambiguously determined is:

$$v_u = \frac{(PRF)\lambda}{4} = \frac{(PRF)c}{4f} \tag{3.8}$$

Combining equations (3.6) and (3.8) gives the following relationship:

$$v_u = \frac{c^2}{8fr_u} = \frac{\lambda c}{8r_u} \tag{3.9}$$

Equation (3.9) shows that in order to maximize r_u, the PRF must be low, and to maximize v_u the PRF must be high. A compromise is necessary if both r_u and v_u are to be measured unambiguously. This is known as the Doppler dilemma and places a fundamental constraint on radar design if a constant PRF is used.

2. Power Received

Another primary quantity measured by the radar is the received power. Following Raghaven (2003), consider a radar antenna to be an isotropic point radiator radiating equally in all directions with a power, P_t, in Watts. At a given distance, r, power is spread informally over the surface area, $4\pi r^2$, of a sphere. The power incident on a unit area or power density is:

$$\frac{P_t}{4\pi r^2} \tag{3.10}$$

Because the antenna is directional, it transmits power in a given sector. This is referred to as G, or antenna gain, and is the ratio of power a directional antenna transmits in the sector to the power an isotropic antenna would transmit in the same sector. This gives the power density, S_i, at range r as:

$$S_i = \frac{P_t G}{4\pi r^2} \tag{3.11}$$

Assume a target at range r presents an effective area σ to the transmitted radiation and that σ is small compared to the area of the radar beam. The target intercepts a power σS_i, which, if radiated isotropically, would produce a power density at the receiving antenna equal to that actually received from the target. The σ that satisfies this condition is referred to as the radar cross section of the target. The power re-radiated from the target towards the antenna is:

$$\frac{P_t G \sigma}{(4\pi r^2)} \tag{3.12}$$

This re-radiated power will spread uniformally over the surface of a sphere of radius r so, for a monostatic radar, the power density at the radar receiver is

$$\frac{P_t G \sigma}{(4\pi r^2)^2}. \tag{3.13}$$

If the effective aperture area of the antenna is A_e, the power received by the radar, P_r, is:

$$P_r = \frac{P_t G A_e \sigma}{(4\pi r^2)^2} \tag{3.14}$$

From antenna theory (Kraus 1950) it can be shown that:

$$A_e = \frac{G\lambda^2}{4\pi} \tag{3.15}$$

Therefore,

$$P_r = \frac{P_t G^2 \lambda^2 \sigma}{(4\pi)^3 r^4}. \tag{3.16}$$

When P_r equals the Minimum Detectable Signal, S_{min}, of the receiver, it represents the maximum range of the radar. This fundamental relationship is known as the Radar Range Equation (RRE):

$$r_{\max} = \left(\frac{P_t G^2 \sigma \lambda^2}{(4\pi)^3 S_{\min}} \right)^{1/4} \tag{3.17}$$

The RRE shows that for a target small in relation to the radar beam area, the received echo power is inversely proportional to the fourth power of the range.

3. Noise and Integration

Radars can detect echo power levels on the order of 10^{-17} of the transmitted power. Because these signals are so weak, the performance of the radar receiver is limited not by its amplification but by the noise figure of the receiving system. This noise figure, N_o, is expressed in Kelvin but is not a physical temperature. It consists of the antenna noise temperature, T_a, and the equivalent receiver noise temperature, T_e and is expressed as

$$N_o = k(T_A + T_E)B_N \tag{3.18}$$

where k = Boltzman's constant, 1.38 x 10^{-23} J/K and B_n = noise bandwidth in Hz. In the presence of noise, the key parameter for detection of the radar echo is the Signal to Noise

Ratio (SNR). SNR is expressed as the power received, P_r, divided by the noise, N. From equation (3.16) the SNR is:

$$SNR = \frac{p_r}{N_o} = \frac{P_t G^2 \lambda^2 \sigma}{(4\pi)^3 r^4 N_o} \tag{3.19}$$

Equivalently, solving equation (3.17) for r_{max} in terms of SNR gives:

$$r_{\max} = \left(\frac{P_t G^2 \sigma \lambda^2}{(4\pi)^3 N_o S_{\min}} \right)^{1/4} \tag{3.20}$$

Integrating the return of n pulses will improve the SNR. For Doppler radar, coherent integration of n samples, which preserves the phase information of the return echoes, improves the SNR by a factor of n. If two correlated pulses are integrated, their signal voltage combines in phase and doubles while the noise voltage combines with random phase and remains unchanged. This produces an improvement of two in the SNR. If n pulses are coherently integrated, the improvement in SNR is ideally:

$$SNR_n = n \times SNR_1 \tag{3.21}$$

The integration improvement factor is defined as:

$$I_i(n) = \frac{SNR_n}{SNR_1} = nE_i(n) \tag{3.22}$$

where $E_i(n)$ = an efficiency factor accounting for less than perfect integration. Utilizing equation (3.22), the RRE (3.20) can be rewritten to include integration of returns from n pulses:

$$r_{\max} = \left(\frac{P_t G^2 \sigma \lambda^2 n E_i(n)}{(4\pi)^3 N_o SNR_1} \right)^{1/4} \tag{3.23}$$

where SNR_1 = the SNR for single pulse detection. In RRE (3.23), P_t is the peak pulse power. The radar duty cycle, τ / T_p, is the fraction of the interpulse period that the pulse is on. Figure 3.3 shows this relationship.

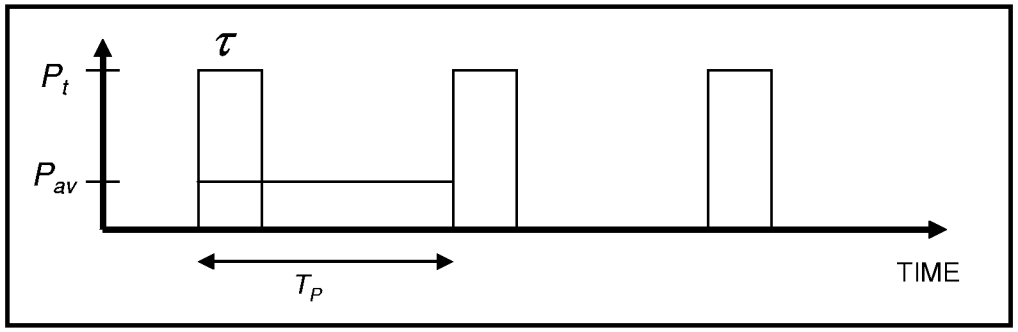

Figure 3.3. Peak and average power (After Knorr and Jenn 2004).

P_{av} is average power computed as if the pulse energy, $P_t\tau$, were spread over the entire interpulse period, T_p:

$$P_{av} = \frac{P_t\tau}{T_p} = P_t\tau(PRF) \tag{3.24}$$

Utilizing equation (3.24), when n pulses are integrated, P_{av}, based on n pulses, should be used in RRE (3.23):

$$r_{\max} = \left(\frac{P_{av}G^2\sigma\lambda^2 nE_i(n)}{(4\pi)^3 N_o SNR_1 \tau(PRF)} \right)^{1/4} \tag{3.25}$$

4. Power Received from Meteorological Targets

Thus far, RRE (3.25) shows the maximum range based on a single target. The meteorological target, however, consists of an ensemble of many small targets such as cloud or raindrops that fill the volume of the radar pulse at any given instant. Each particle back-scatters some energy and therefore has a certain back-scattering cross section. If one assumes the scattering is incoherent, i.e., the particles are randomly distributed in the volume and their individual echo phases are distributed over a 2π interval, then the expected value of the total back-scattering cross section is the sum of the expected values of the individual cross sections. The radar cross-section, RCS, for volume targets is defined in terms of the radar cross-section density, η, in units of cm^2/m^3 (RCS per unit volume). The radar cross-section density multiplied by the volume illuminated by the radar pulse gives the total radar cross section of the volume. For Rayleigh scattering, the back-scattering cross section, σ, of a single spherical drop of diameter D is:

$$\sigma = \left(\frac{\pi^5}{\lambda^4}\right) \times |K|^2 \times D^6 \tag{3.26}$$

where: $|K|^2$ $= (\varepsilon_r - 1)/(\varepsilon_r + 2)$ and ε_r is the complex dielectric constant

ε_r $\cong 80$ for water and $\cong 4.2$ for ice

If the scattering volume contains drops of various sizes, the sixth powers of the diameters of the individual drops are summed up over a unit volume to obtain the expected value of the cross-section density, $E(\eta)$:

$$E(\eta) = \left(\frac{\pi^5}{\lambda^4}\right) \times |K|^2 \times \frac{1}{V} \sum_{i=1}^{n} D^6{}_i \; m^2 / m^3 \tag{3.27}$$

Reflectivity, Z, is defined as

$$Z = \frac{1}{V} \sum_{i \in V} D_i^6 \tag{3.28}$$

and is conventionally expressed using units of mm^6/m^3. It is a property solely of the volume of particles and is independent of the radar wavelength if $\pi D/\lambda < 1$.

In general, radiation from a parabolic dish antenna travels out in the shape of a cone. Power spreads out over a finite angular width on either side of the direction of maximum radiation. The angle between the two directions on either side of the maximum where the power density is half of the maximum defines the 3 dB beam width of the antenna. Assume the beamwidth, ϕ, in the vertical and horizontal planes are the same, i.e. defining a cone, the beam at range r spreads out over an area equal to,

$$\pi \times \left(\frac{r\phi}{2}\right)^2 \tag{3.29}$$

neglecting any radiation transmitted outside the beamwidth. At any instant, the traveling radar pulse will occupy a finite range interval, r to $r+h$, with $h=c\tau$ being the pulse width. Back-scattered power from the particles at a range $r+h/2$ from the front of the outgoing pulse will arrive at the radar with time delay τ (pulse width) relative to the power scattered by particles at range r. This defines the effective range resolution or the ability

of the radar to differentiate between targets at the same angle but different ranges. Thus the volume sampled by the radar at any instant is:

$$V = \pi \times \left(\frac{r\phi}{2}\right)^2 \times \left(\frac{c\tau}{2}\right) \tag{3.30}$$

where ϕ is normally taken to be the two-way 3 dB beamwidth. The expected value of the total radar cross section of the particles in the volume is

$$\sigma = \eta \times V. \tag{3.31}$$

Substituting equation (3.31) in equation (3.16) gives the expected value of the total power received by the radar from the sample volume:

$$E[P_r] = \frac{P_t c\tau G^2 \lambda^2 \phi^2 E[\eta]}{512\pi^2 r^2} \tag{3.32}$$

Probert-Jones (1962) gave a more accurate form of the radar equation for meteorological targets that accounts for beam shape as

$$E[P_r] = \frac{P_t c\tau G^2 \lambda^2 \phi^2 E[\eta]}{1024(\ln 2)\pi^2 r^2}. \tag{3.33}$$

Substituting for $E[\eta]$ from equation (3.27) gives $E[P_r]$ as a function of Z:

$$E[P_r] = \frac{P_t c\tau G^2 \phi^2 \pi^3 |K|^2 Z}{1024(\ln 2)\lambda^2 r^2} \tag{3.34}$$

This shows that reflectivity, Z, can be estimated using average backscattered power.

B. SPECTRAL MOMENTS

1. Introduction

Because meteorological targets consist of millions of individual scatterers or raindrops in each radar resolution cell, the weather signal must be modeled statistically. Within each sample volume or resolution cell, individual scatterers are moving with respect to each other and at the same time the ensemble itself may be moving as a result of larger scale air motions. The back scattered signal thus contains information about the

velocities of the individual scatterers in the form of a spectrum of Doppler shift frequencies (Raghaven 2003). The total power, P_r, received by the radar is the sum of the individual contributions of all the particles in the sample volume taking into account the echo phase of each particle. The reflectivity or zeroth moment of the Doppler power spectrum is found from the time average power of the weather signal backscattered from the ensemble, Eq. (3.34). The Doppler frequency shift or first moment of the Doppler power spectrum of a weather signal can be found from the RF carrier phase shift induced by ensemble radial velocity. Over time, the weather signal phase shift (velocity) exhibits a spread due to turbulence, wind shear and terminal velocity differences for drops of different sizes. This spread is called the variance or second moment of the Doppler power spectrum and its square root is called the root mean square spectrum width.

2. Gaussian Distribution of Meteorological Targets

It can be shown that the received signal from meteorological targets is well represented by a Gaussian statistical process (Skolnik 1990). For example, a rain return consists of the returns from a large number of small scatterers. Figure 3.4 shows how the return power from rain varies with time. $\overline{P}$ indicates the average of the signal and T_s indicates sampling time.

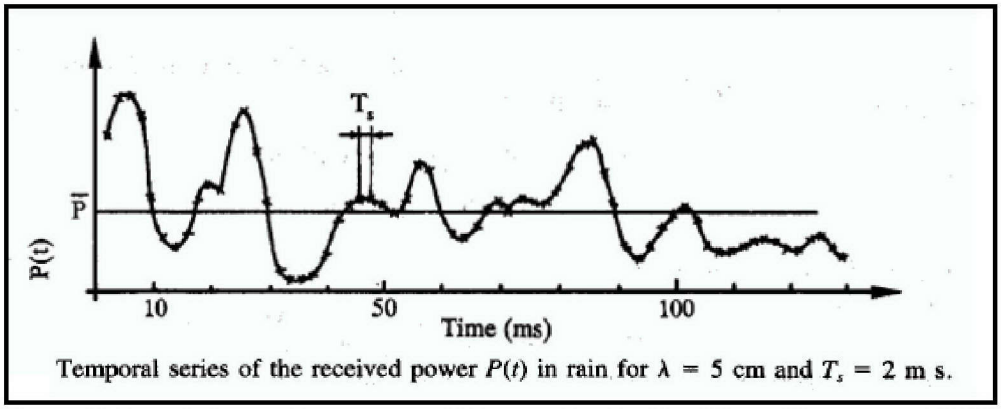

Figure 3.4. Fluctuating power of the received echo (From Sauvageot 1992).

As stated earlier, the total instantaneous power, P_r, received by the radar is the sum of the individual contributions of all the particles in the sample volume taking into account the echo phase of each particle. To get a representative value of the average backscattered power, it is necessary to average the fluctuating signal over a long enough period of time. The $\overline{P}$ or $\overline{P}_r$ symbol is used to indicate this averaging. Following

Sauvageot (1992), in order to get a measure of the reflectivity, P_r, or mean power, a number of independent or uncorrelated samples must be averaged or integrated. The average of k independent samples of the instantaneous power is:

$$J_k = k^{-1}\sum_{i=1}^{k} P_i \tag{3.35}$$

The probability density function, $P(J_k)$, from Marshall and Hitschfeld (1953) is,

$$P(J_k) = \frac{k^k}{\overline{P}^k (k-1)!} J_k^{k-1} e^{-kJ_k/\overline{P}} \tag{3.36}$$

with a standard deviation of $\overline{P}/k^{1/2}$. This function is shown in Figure 3.5 for various values of k. For k greater than 10, the distribution is nearly Gaussian. As k increases, the distribution becomes more peaked and narrow because averaging more samples results in an estimate that has a higher probability of being close to the true value of average power.

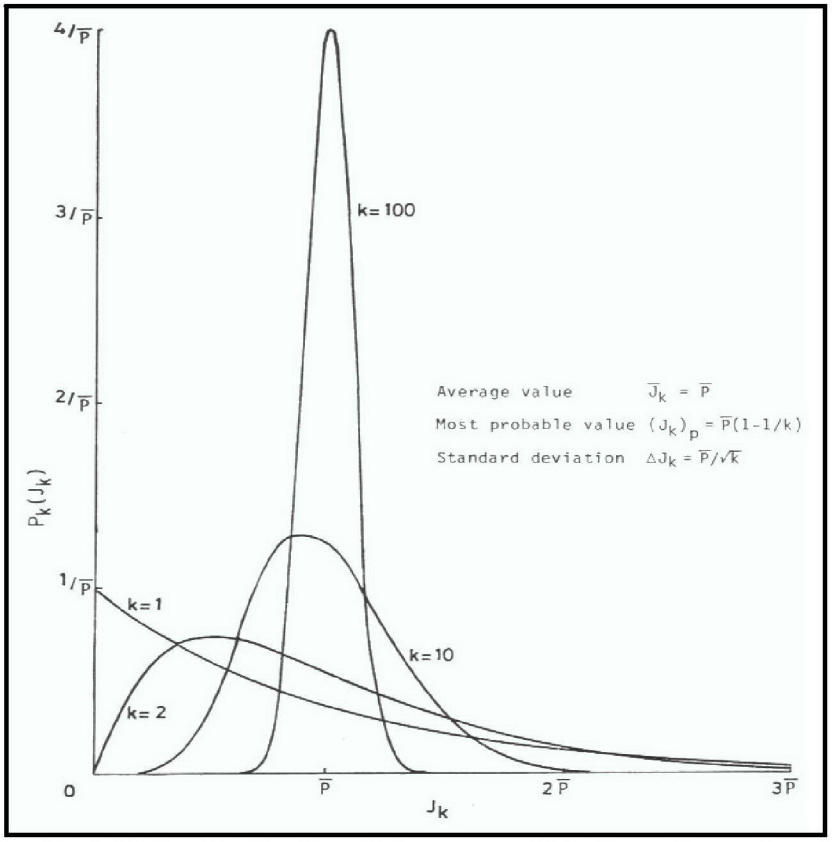

Figure 3.5. Probability distribution of the mean of k independent values of the signal power when average power is $\overline{P}$ (From Marshall and Hitschfeld 1953).

The curves in Figure 3.6 are computed from equation (3.36) and show the limits below which the indicated percentages of the averages of k independent samples are expected to fall. For example, when k = 30, 10% of the averages are below 0.75 $\overline{P}$ and 90% below 1.25 $\overline{P}$. This means the 80% confidence limits are $\overline{P} \pm 0.25\ \overline{P}$. These particular limits correspond to + 1 dB to – 1.3 dB and are close to the desired instrument accuracy in the measurement of $\overline{P}$. These results provide a way to determine the duration of the observations necessary to arrive at an estimate with a given accuracy (Sauvageot 1992).

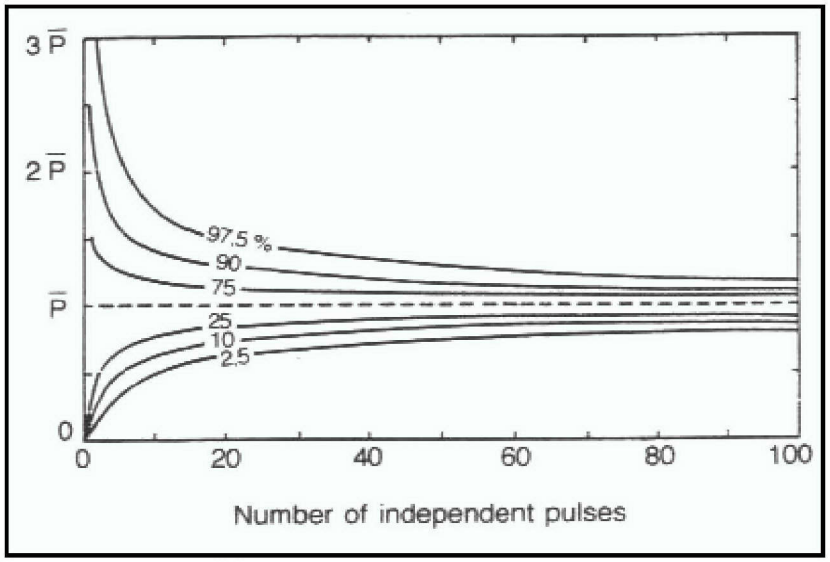

Figure 3.6. Estimation of $\overline{P}$ as a function of the number of independent pulses used to calculate the average (From Marshall and Hitschfeld 1953).

3. The Doppler Spectrum

The echo arriving from a given sample volume is considered to be the sampling of a Gaussian process and its amplitude, *y(t)*, which is a complex random function of time described by statistical properties, is given as

$$y(t) = A(t)e^{-i\phi(t)} \tag{3.37}$$

where A = signal amplitude and ϕ = signal phase. The spectral density function, *Y(f)*, defines the amplitude spectrum and is the Fourier transform of the complex signal. For a continuous, steady-state process it is given by

$$Y(f) = \int_{-\infty}^{+\infty} y(t)e^{-i2\pi ft}dt, \tag{3.38}$$

and its corresponding power spectral density is

$$S'(f) = |Y(f)|^2 . \tag{3.39}$$

The power spectral density can also be obtained from the complex autocorrelation function, $R(\tau)$, which is defined by

$$R(\tau) = \lim_{T\to\infty} \frac{4}{T} \int_{-T/2}^{T/2} y(t)\, y^*(t+\tau)\, dt \tag{3.40}$$

where τ = the autocorrelation interval and y^* = the complex conjugate quantity. $S'(f)$ is the Fourier transform of $R(\tau)$:

$$S'(f) = \int_{-\infty}^{+\infty} R(\tau) e^{-i2\pi f\tau} d\tau. \tag{3.41}$$

Transform (3.41) also has the associated reciprocal transform

$$R(\tau) = \int_{-\infty}^{+\infty} S'(f) e^{i2\pi f\tau} df. \tag{3.42}$$

The distribution of $S'(f)$ as a function of frequency describes the Doppler spectrum. The power in a frequency interval between f and $f + df$ is $p(f) = S'(f)df$. The summation of $S'(f)$ over the entire spectrum gives the average received power or zeroth moment of the spectrum as

$$\overline{P}_r = \int_{-\infty}^{+\infty} S'(f) df. \tag{3.43}$$

$\overline{P}_r$ is a primary characteristic of the Doppler spectrum, and is shown as the area under the curve in Figure 3.7a. By convention, the power spectral density is normalized by the average received power, $S(f)=S'(f)/P_r$, which is also the probability density of the distribution. Statistical moments of order n to $S(f)$ are associated by the general expression

$$m_n = \int_{-\infty}^{+\infty} f^n S(f) df. \tag{3.44}$$

Two other primary characteristics of the Doppler spectrum, shown in Figure 3.7a, are the average frequency, $\overline{f}$, and the variance, σ_f^2, which are written as

$$\bar{f} = \int_{-\infty}^{+\infty} f S(f) df = m_1, \tag{3.45}$$

$$\sigma_f^2 = \int_{-\infty}^{+\infty} (f - \bar{f})^2 S(f) df = \bar{f^2} - (\bar{f})^2 = m_2 - m_1^2. \tag{3.46}$$

The average frequency, $\bar{f}$, is the first moment of the normalized spectrum and the variance, σ_f^2, is the second central moment (centered with respect to the mean) of the normalized spectrum. The standard deviation, σ_f, is the square root of the variance, σ_f^2, and is a measure of the spectrum width. The width of the spectrum arises because of the spread of relative velocities of the particles in the radial direction. The observed velocity spread is due to (Doviak and Zrnic 1993): 1) turbulence, σ_t, 2) wind shear, σ_s, 3) differences in fall velocities, σ_d, due to drop size distribution, and 4) antenna motion, σ_a. Radar antenna motion can corrupt velocity measurement by inducing a frequency spread resulting from the finite observation time and care must be taken to minimize this effect. Assuming independent Gaussian processes, the variance or square of the spectrum width is the sum of these four contributions:

$$\sigma_v^2 = \sigma_t^2 + \sigma_s^2 + \sigma_d^2 + \sigma_a^2. \tag{3.47}$$

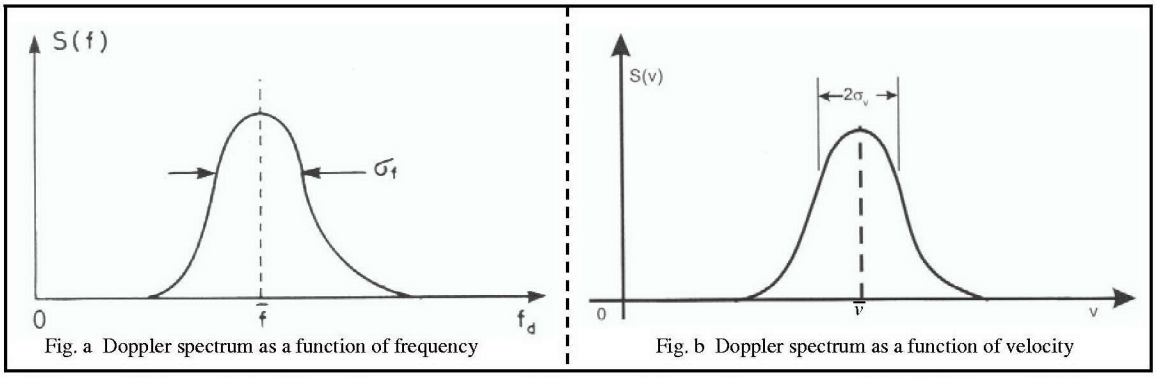

Fig. a Doppler spectrum as a function of frequency

Fig. b Doppler spectrum as a function of velocity

Figure 3.7. The Doppler spectrum (Figure a From Sauvageot 1992, Figure b From Skolnik 1990).

The velocity spectrum is the image of the frequency spectrum therefore

$$S(f)df = S(V)dV. \tag{3.48}$$

The preceding equations can be transposed in terms of velocity by the following relationships between velocity and frequency:

$$\bar{V} = -\frac{\lambda}{2}\bar{f}, \tag{3.49}$$

$$\sigma_v^2 = \frac{\lambda^2}{4}\sigma_f^2. \tag{3.50}$$

Figure 3.7b illustrates the Doppler spectrum as a function of velocity. Skolnik (1990) gives the three moments of the Doppler spectrum in terms of velocity. Power, P_r, is given by

$$P_r = \int_{-\infty}^{+\infty} S(f)df = \int_{-\infty}^{+\infty} S(v)dv \tag{3.51}$$

where f and v are related by

$$f = \left(\frac{2}{\lambda}\right)v. \tag{3.52}$$

Mean velocity, $\bar{v}$, and spectrum width, σ_v, in are given as

$$\bar{v} = \frac{\int_{-\infty}^{+\infty} vS(v)dv}{\int_{-\infty}^{+\infty} S(v)dv}, \tag{3.53}$$

$$\sigma_v = \left(\frac{\int_{-\infty}^{+\infty} (v-\bar{v})^2 S(v)dv}{\int_{-\infty}^{+\infty} S(v)dv}\right)^{1/2}. \tag{3.54}$$

4. Meteorological Moment Estimators

A single sample of a weather signal gives instantaneous power and velocity. A number of samples are required to estimate average power, average velocity and velocity spread. Consequently, the estimates of the weather signal parameters are found by averaging with the number of samples determined by the desired accuracy (variance) for each of the estimates. Typically, the accuracies sought are ±1 dBZ for reflectivity and ±1 m/s for velocity and spectrum width. In the radar receiver, the output from the coherent detector is a complex signal containing both amplitude and phase information. This signal is decomposed into two vector components, in-phase, I, and quadrature, Q, having a phase difference of 90° that, when added vectorally, form the complex signal.

The moment estimators are developed following Knorr and Jenn (2004) and assume high SNRs for the weather signals of interest in this work.

Return power is estimated from a combination of time (pulse to pulse) and range (adjacent sample volume) averaging. Rewriting equation (3.34) for reflectivity, Z, in terms of the average received weather echo signal power gives

$$Z = \left[\frac{P_t c \tau G^2 \phi^2 \pi^3 |K|^2}{1024(\ln 2)\lambda^2 r^2} \right]^{-1} \overline{P}_r. \tag{3.55}$$

Given N independent samples of echo power, the reflectivity estimator is given by

$$\hat{Z} = Const \times \frac{1}{N} \sum_{n=1}^{N} |Z_n|^2 = Const \times \frac{1}{N} \sum_{n=1}^{N} \left[|I_n|^2 + |Q_n|^2 \right]. \tag{3.56}$$

From Eq. (3.36), it follows that the standard deviation of the reflectivity estimate is

$$\sigma_{\hat{Z}} = \frac{\hat{Z}}{\sqrt{N}}. \tag{3.57}$$

Mean velocity estimates are made by a technique that estimates the first moment of the spectral density from the argument of the complex covariance. Because, the complex covariance and spectral density constitute a Fourier transform pair, the spectral density moments correspond to the complex covariance evaluated at zero lag. This technique is referred to as pulse pair processing. The output from the coherent detector is

$$\left.\begin{aligned} I_n &= A_n \cos\left[\frac{4\pi R_n}{\lambda} - \psi \right] \\ Q_n &= A_n \sin\left[\frac{4\pi R_n}{\lambda} - \psi \right] \end{aligned}\right\} Z_n = I_n + jQ_n = A_n e^{j\left[\frac{4\pi R_n}{\lambda} - \psi\right]} = A_n e^{j\theta_n}, P_n = Z_n Z_n^* \tag{3.58}$$

where Z^* = complex conjugate of Z, and

$$\frac{\lambda}{4\pi} \frac{(\theta_{n+1} - \theta_n)}{T_s} = \frac{(R_{n+1} - R_n)}{T_s} = v_{n+1}. \tag{3.59}$$

Thus the arguments of sample pairs, Z_n and Z_{n+1}, can be used to estimate the velocity. The average or mean velocity estimate comes from processing pairs of correlated pulses. From a single, correlated pulse pair, the velocity is calculated from

$$Z_{n+1}Z_n^* = |Z_{n+1}||Z_n| \angle(\theta_{n+1} - \theta_n), \tag{3.60}$$

where $\angle$ is the angle between $(\theta_{n+1} - \theta_n)$ and

$$Arg\left\{\frac{Z_{n+1}Z_n^*}{|Z_{n+1}||Z_n|}\right\} = (\theta_{n+1} - \theta_n). \tag{3.61}$$

Therefore, the velocity estimator for a single pulse pair is

$$v_{n+1} = \frac{\lambda}{4\pi}\frac{(\theta_{n+1} - \theta_n)}{T_s} = \frac{\lambda f_p}{4\pi}(\theta_{n+1} - \theta_n) = \frac{\lambda f_p}{4\pi} Arg\left\{\frac{Z_{n+1}Z_n^*}{|Z_{n+1}||Z_n|}\right\} \tag{3.62}$$

where f_p=*PRF*. Given N independent sample pairs, the velocity estimator is

$$\hat{v} = \frac{1}{N-1}\sum_{n=1}^{N-1} v_{n+1} = \frac{1}{N-1}\frac{\lambda f_p}{4\pi}\sum_{n=1}^{N-1} Arg\left\{\frac{Z_{n+1}Z_n^*}{|Z_{n+1}||Z_n|}\right\}. \tag{3.63}$$

For large SNR, narrow spectrum widths, and contiguous pairs, Doviak and Zrnic (1993) give the accuracy or variance, $\mathrm{var}(\hat{v})$, for mean Doppler velocity as

$$\mathrm{var}(\hat{v}) \approx \frac{\sigma_v \lambda}{8MT_s\sqrt{\pi}} \tag{3.64}$$

where, σ_v = signal spectrum width, λ = radar wavelength, M = number of samples, and T_s = sample time.

Spectrum width estimates are computed by signal autocorrelation because signal correlation and power spectral density constitute a Fourier transform pair. For weather signals with a Gaussian distribution, the autocorrelation coefficient, $\rho(\tau)$, is

$$\rho(\tau) = e^{-\left(\frac{\tau^2}{2(\pi\sigma_f)^2}\right)} = e^{-\left[8\left(\frac{\pi\sigma_v\tau}{\lambda}\right)^2\right]}. \tag{3.65}$$

Taking the log of both sides gives

$$\ln\rho(\tau) = -\left[8\left(\frac{\pi\sigma_v\tau}{\lambda}\right)^2\right]. \tag{3.66}$$

Solving for root mean square (rms) velocity spread with $\tau = T_s$, gives the spectral width estimator as

$$\hat{\sigma}_v = \frac{\lambda}{2\sqrt{2}\pi T_s}\left|\ln \rho(T_s)\right|^{1/2}. \tag{3.67}$$

For large SNR and contiguous pairs, Doviak and Zrnic (1993) give the accuracy or variance, $\mathrm{var}(\hat{v})$, of the spectrum width as

$$\mathrm{var}(\hat{\sigma}_v) \approx \left(\frac{3\lambda^2}{128\sqrt{\pi}MT_s^2}\right)\sigma_{vn} \tag{3.68}$$

where, σ_{vn} is the normalized unambiguous velocity interval,

$$\sigma_{vn} = \frac{2\sigma_v T_s}{\lambda}. \tag{3.69}$$

5. Correlation and Coherency

The accuracy or variance of the parameter estimates, $\hat{Z}$, $\hat{v}$, and $\hat{\sigma}_v$, depends in general on the number and correlation of the samples used to derive the estimates. To obtain uncorrelated samples, the sample time (ref. Figure 3.4) must be long enough to allow the ensemble of scatterers to reshuffle into an independent configuration. This implies a low PRF or alternatively, sampling at a different frequency to collect uncorrelated samples. For velocity, $\hat{v}$, or spectrum width, $\hat{\sigma}_v$, estimates, contiguous coherent or correlated samples are required. That is, the sample time of subsequent echoes must be sufficiently small so that the ensemble of scatterers does not reshuffle into an independent configuration. High coherency provides a mean value of Doppler frequency shift or mean velocity (ref. Figure 3.7). This high sample correlation similarly provides the measure of deviation about the mean or the spectrum width. The velocity spread determines correlation and coherency.

The time, τ, that must elapse in order to obtain independent samples comes from the autocorrelation function. From Sauvageot (1992), assuming Gaussian power spectral density,

$$S(f) = S_0 e^{-f^2/2\sigma_f^2}. \tag{3.70}$$

The normalized autocorrelation function $R(\tau)$ from the Fourier transform of $S(f)$ can be written as

$$R(\tau) = e^{-\tau^2/2\sigma_\tau^2} \tag{3.71}$$

where σ_τ^2 = the variance of the autocorrelation function, with

$$\sigma_\tau = (2\pi\sigma_f)^{-1}. \tag{3.72}$$

Utilizing equation (3.50), equation (3.71) can be rewritten as equation (3.65):

$$\rho(\tau) = e^{-\left(\frac{\tau^2}{2(\pi\sigma_f)^2}\right)} = e^{-\left[8\left(\frac{\pi\sigma_v\tau}{\lambda}\right)^2\right]}. \tag{3.73}$$

where $R(\tau) = \rho(\tau)$. The value of $\rho(\tau)$ decreases more quickly with τ, from 1, when σ_v is high. Samples are normally assumed independent when $\rho(\tau) \leq 0.02 \approx e^{-4}$. This defines the decorrelation time, τ_i. From equation (3.73) the decorrelation time is

$$\tau_i = \frac{\lambda}{\sqrt{2}\pi\sigma_v} \approx \frac{\lambda}{5\sigma_v} \tag{3.74}$$

where λ is in mm, σ_v is in m/s, and τ is in ms. From this, the lower bound on sample time, T_s, for decorrelated samples is:

$$T_s \geq \frac{\lambda}{\sqrt{2}\pi\sigma_v} \approx \frac{\lambda}{5\sigma_v} \tag{3.75}$$

The lines of Figure 3.8 from equation (3.74) shows how τ_i varies with σ_v for several values of λ. The figure shows that for a given wavelength, τ_i decreases with increasing σ_v. For a fixed σ_v, τ_i decreases with shorter wavelengths.

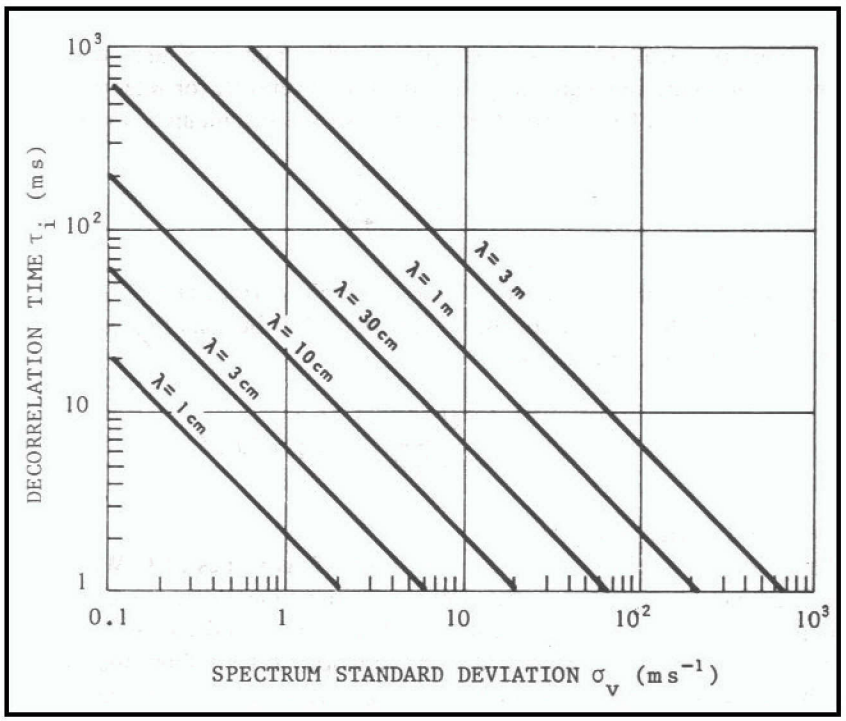

Figure 3.8. Independent sampling time versus spectrum width (From Sauvageot 1992).

Conversely, in order to obtain correlated or coherent sample pairs for velocity estimation, the sample time, T_s, must be sufficiently short. Equality (high correlation) occurs if the normalized correlation function $\rho(T_s)=e^{-1/2}$ or $\rho \approx 0.6$. From this threshold, the upper bound on sample time, T_s, as well as unambiguous range, r_u, can be calculated as:

$$T_s \leq \frac{\lambda}{4\pi\sigma_v} \tag{3.76}$$

$$r_u \leq \frac{c\lambda}{8\pi\sigma_v} \tag{3.77}$$

Figure 3.9 shows how σ_v varies with r_u for several values of λ. The figure clearly shows that for shorter wavelength radars, a large unambiguous range cannot be achieved unless the rms velocity spread of the weather signal is small. In general, weather signals of interest will not have small rms velocity spread and the short sample times required to obtain large unambiguous velocity results in a range ambiguity problem at low elevation angles (longer ranges).

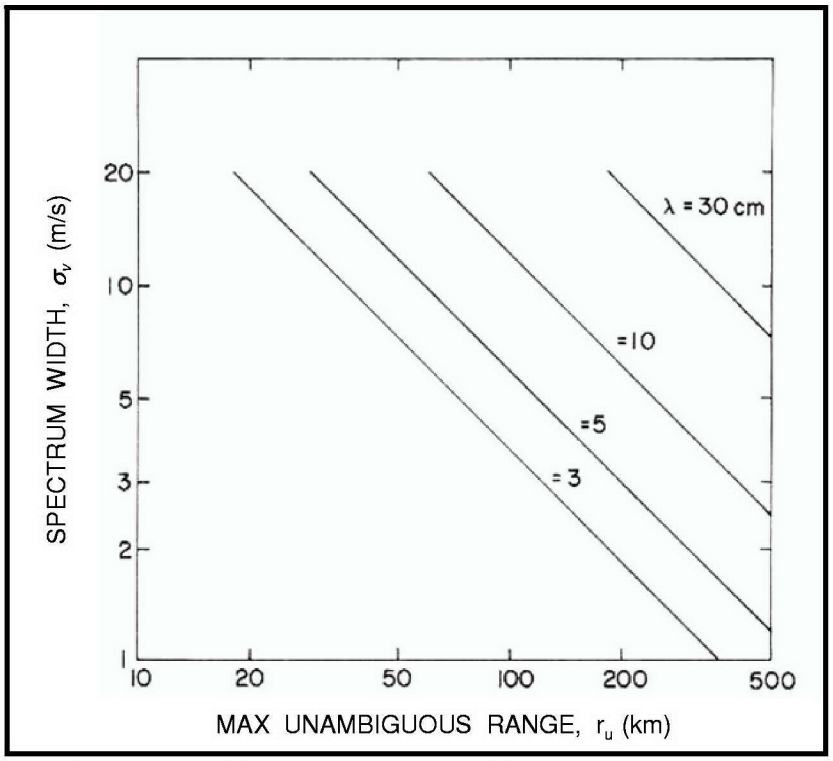

Figure 3.9. Spectrum width versus max unambiguous range for correlated samples (After Doviak and Zrnic 1993).

THIS PAGE INTENTIONALLY LEFT BLANK

IV. PROPOSED SCANNING STRATEGIES FOR RESEARCH APPLICATIONS

Knowledge of the spectrum width of various weather phenomena is essential to the approach utilized in this chapter for development of sampling requirements. For clarity, the terms radar and MWR-05XP are used interchangeably in this chapter. A brief review of Fang and Doviak's (2001, hereafter FD 2001) method of obtaining reliable spectrum width data from the WSR-88D is first presented. The spatial and temporal sampling scales of isolated supercell tornadic storms and non-supercell severe storm clusters (multicellular storms) are developed next. The desired accuracy (variance) of the meteorological parameters will be presented. The number of samples required to achieve the desired accuracy, along with the weather phenomena spectrum widths and sampling scales, will be used to develop sampling strategies based on the known capabilities of the MWR-05XP. Unique features of the MWR-05XP utilized to increase the scanning rate include frequency shift and frequency backscan along with phase shift scanning techniques. Proposed sampling schemes will need to be coded and programmed into the WRP for testing when the MWR-05XP is delivered at contract completion.

A. RELATING SPECTRUM WIDTH DATA TO VARIOUS WEATHER CONDITIONS

The use of spectrum width data has been very limited compared to reflectivity and Doppler velocity data. This is due in part to relating spectrum width, σ_v, to meteorologically significant phenomena, and in part to the fact that σ_v is easily corrupted by WSR-88D radar artifacts which make the data unreliable and risky to interpret (FD 2001). This section discusses how reliable spectrum width data was obtained from WSR-88D observations. The derived spectrum width values from FD 2001 applicable to research applications are: a) less than 2.0 m/s for isolated supercells and tornadoes, and b) less than 4.0 m/s for multicellular severe storm clusters. These values, along with the radar operating frequency, sample time, and number of independent samples, are used to develop the phenomena specific sampling requirements and affect the accuracy (variance) of the moment estimates.

1. WSR-88D Spectrum Width Error Sources

Velocity and spectrum width, as observed with the WSR-88D, are estimated using relatively short PRTs which often leads to overlaid (multiple-trip) weather signals that corrupt the measurements. To display a larger area of Doppler velocities, the WSR-88D overlaid threshold has been lowered to 5 dB which increases the number of overlaid weather signals (NEXRAD 1991). Since 1996, the WSR-88D employs a SNR of 3.5 dB instead of the design threshold of 10 dB. Under the lower threshold, a significantly larger standard error for spectrum width of 1.4 m/s is generated instead of the design limit of 1.0 m/s (NEXRAD 1991). Additionally, the algorithms used to estimate spectrum width cause an excessive occurrence of zero width assignments when the noise power is overestimated and true spectrum widths are small. This contaminates all 0 m/s σ_v. Incorrect setup of the Automatic Gain Control (AGC) circuits allows signals to exceed the maximum level of the analog to digital converter. This causes signal clipping which generates harmonics of the weather spectrum in the spectral domain. These harmonics increase the spectrum width values (FD 2001).

2. Censoring Erroneous WSR-88D Spectrum Width Data

To obtain reliable data, WSR-88D spectrum width data was edited for these error sources (FD 2001). Erroneous data was censored by raising the overlaid multiple trip weather signals threshold to 20 dB from 5 dB. If one of the trip signals was 20 dB or more stronger than the sum of the other trip signals, then the spectral moments of the stronger signal were estimated without significant error (within the specifications of the WSR-88D). For the FD 2001 study, algorithms were developed to select data with a signal power at least 20 dB higher than the sum of competing out-of-trip signals. The SNR threshold was raised to 15 dB so that improper noise estimates were much less likely to bias the true spectrum width estimates, especially small width values. Editing the data for correct AGC setup was less quantitative, so data was not classified if a correlation was detected between large echo power levels and large spectrum widths. Together, these editing measures, while censoring large amounts of data which may have contained correct width estimates, insured the data was more accurate and reliable than if less stringent procedures had been employed (FD 2001).

B. SPATIAL AND TEMPORAL SAMPLING SCALES

The spatial and temporal scales to be sampled for the following scenarios are developed, in part, from Bluestein et al. (1993), Doswell (2001), Davies-Jones et al. (2001), and Kessler (1983). Proximity to the weather phenomena to be interrogated is a fundamental consideration. The closer the radar is to the event, the better the meteorological moment estimates will be, however, the total coverage pattern is reduced because of the radar-storm geometry.

1. Isolated Supercell Tornadic Storms

Tornado Doppler wind speeds have been measured as high as 125 m/s (Bluestein et al. 1993) with volumetric updates as fast as 30 seconds (Wurman and Randall 2005). To the author's knowledge, vertical velocities within a tornado funnel have not been directly measured with Doppler radar. From Bluestein et al. (1993), a tornado condensation funnel width of 300 m is assumed at cloud base and ground. The tornado funnel extends from the ground up to cloud base, nominally 1 to 2 km. For tornadic storms, the research goal is to measure wind speeds up to 150 m/s with a volumetric update every 10 seconds. Spectrum width values of $\leq$ 2 m/s for reflectivity between $20 \leq Z \leq 70$ dBZ are assumed from measurements by FD 2001.

To intercept tornadoes, observers attempt to place the radar within 5 km of the storm path. Here the measurement emphasis is on the funnel itself from as close to the ground as possible up to the cloud base. Ideally, the radar should be close enough to allow the beamwidth to resolve the tornado. Figures 4.1 and 4.2 illustrate the radar-storm geometry for a 5 km interception. This geometry was chosen to capture the best horizontal resolution possible at the expense of the height scale. Figure 4.1 shows that the MWR-05XP maximum electronic elevation scan, 22°, allows for measurements from the surface up to 2 km assuming the antenna is not mechanically adjusted in elevation. In Figure 4.2, the radar is not mechanically rotated in azimuth during measurements but is rotated to the centerline of the funnel cloud between sets of measurements. The 7° azimuthal scan is accomplished by frequency scanning through the centerline of the tornado.

Electronic elevation scanning and frequency azimuth scanning were chosen for this sampling scheme because the extremely rapid structural changes in tornadoes (Wurman and Randall 2005) require volumetric updates on the order of 10 seconds. Mechanical azimuth scanning of the antenna during measurements would collect a significant amount of data (in azimuth) not directly associated with the tornado being measured and would slow the volumetric sampling rate.

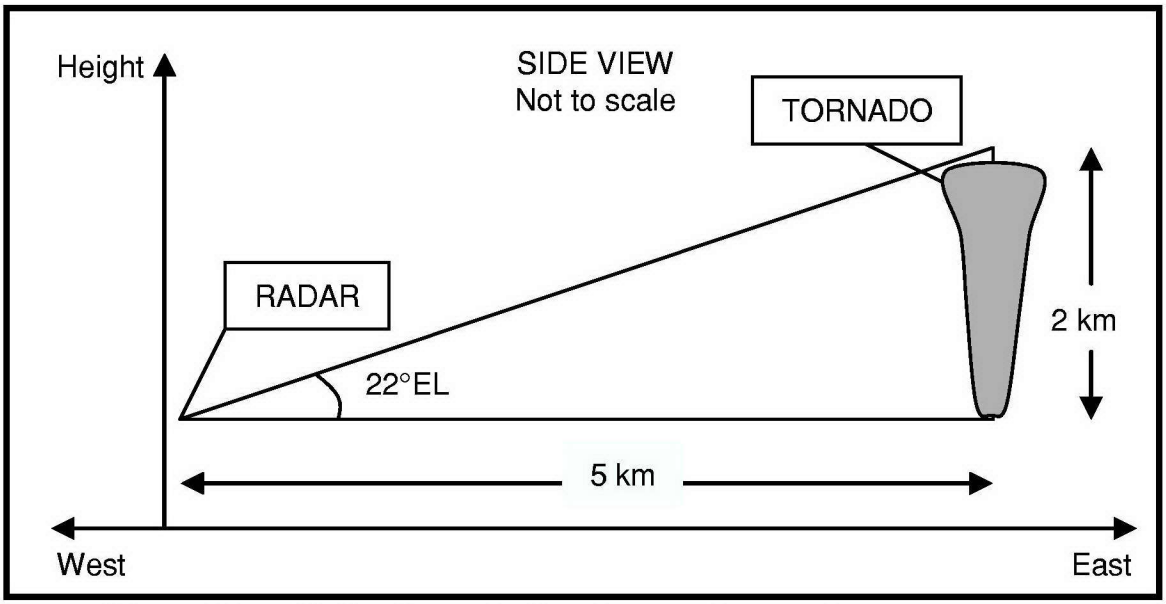

Figure 4.1. Radar electronic elevation scan for tornado measurements.

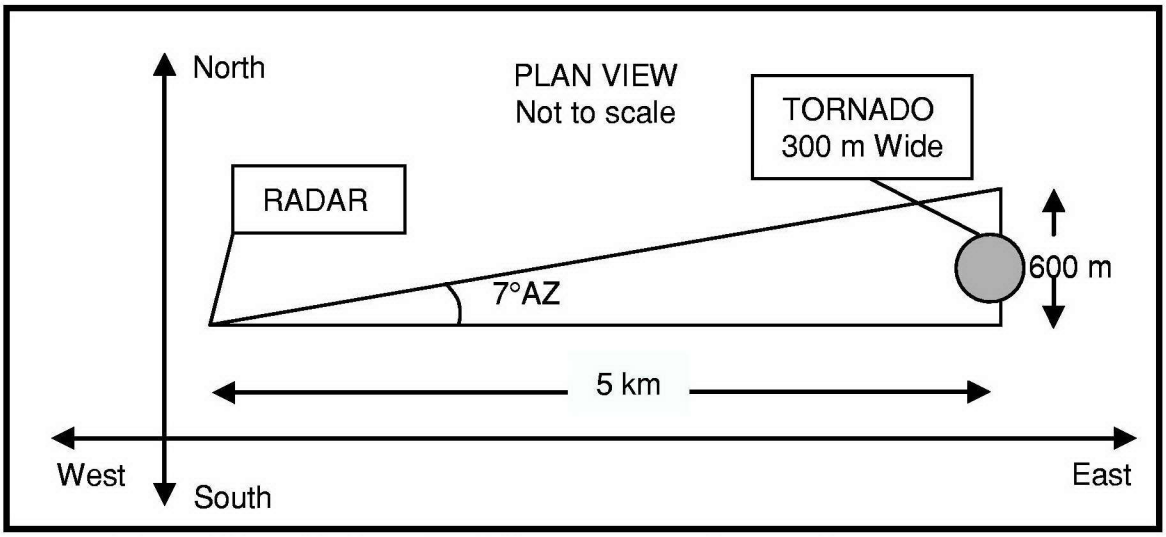

Figure 4.2. Radar azimuth frequency scan for tornado measurements.

2. Multicellular Severe Storm Clusters

The basic building block of multicellular storms is the thunderstorm cell. From Kessler (1983), individual cells average about 8 km wide, with characteristic vertical motions of 10 m/s, and vertical development up to 10 km. An average cluster consists of three to four cells with a horizontal span of about 24 km. For these storms, the research goal is to measure wind speeds up to 75 m/s with a volumetric update every 10 seconds. Spectrum width values of $\leq$ 4 m/s for reflectivity between $20 \leq Z \leq 70$ dBZ are assumed from measurements by FD 2001.

To take measurements in multicellular storms, the radar should be placed 10 km to 20 km from the storm. The measurement emphasis is on individual cells within a multicellular system. Figures 4.3 and 4.4 illustrate typical radar-storm geometry. This particular geometry is a compromise that allows the radar to both capture the scale of an individual cell and provide the best resolution for individual volume samples. Figure 4.3 is a side view and illustrates two 22° electronic elevation scans. This means that the first set of measurements is taken approximately at 0° to 22° elevation before the antenna is mechanically elevated for the second set of measurements from approximately 24° to 46° to capture the height of the cell. Figure 4.4 is a top view and illustrates mechanical 45° azimuth sector scanning to acquire the width of the cell.

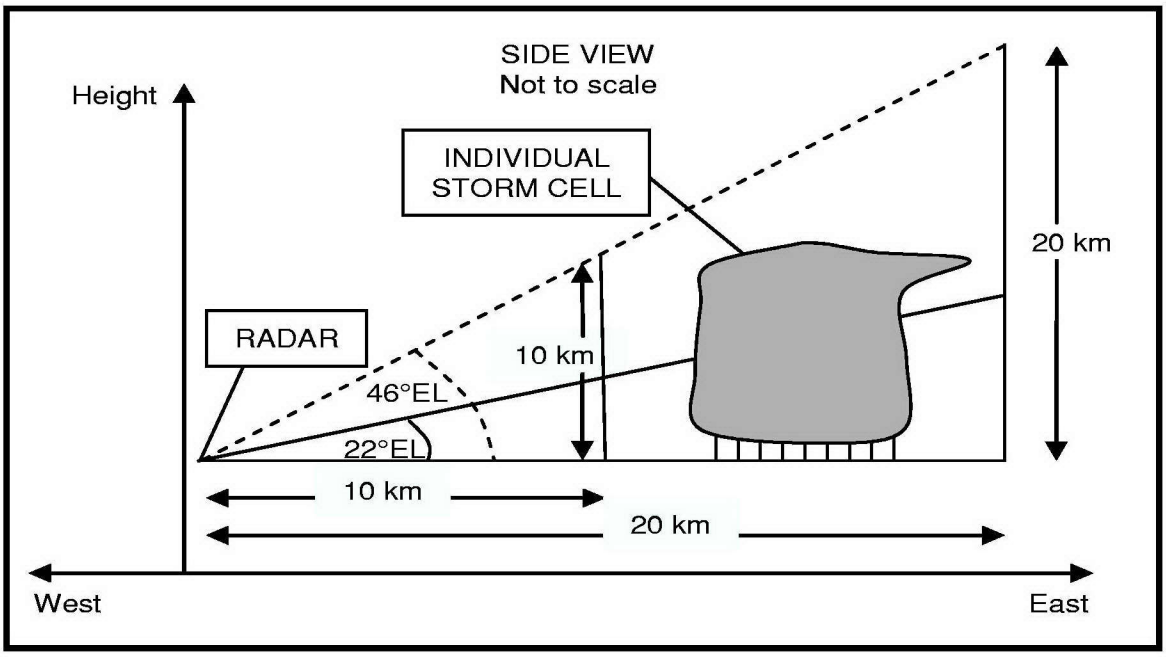

Figure 4.3. Radar electronic elevation scan for multicellular storms.

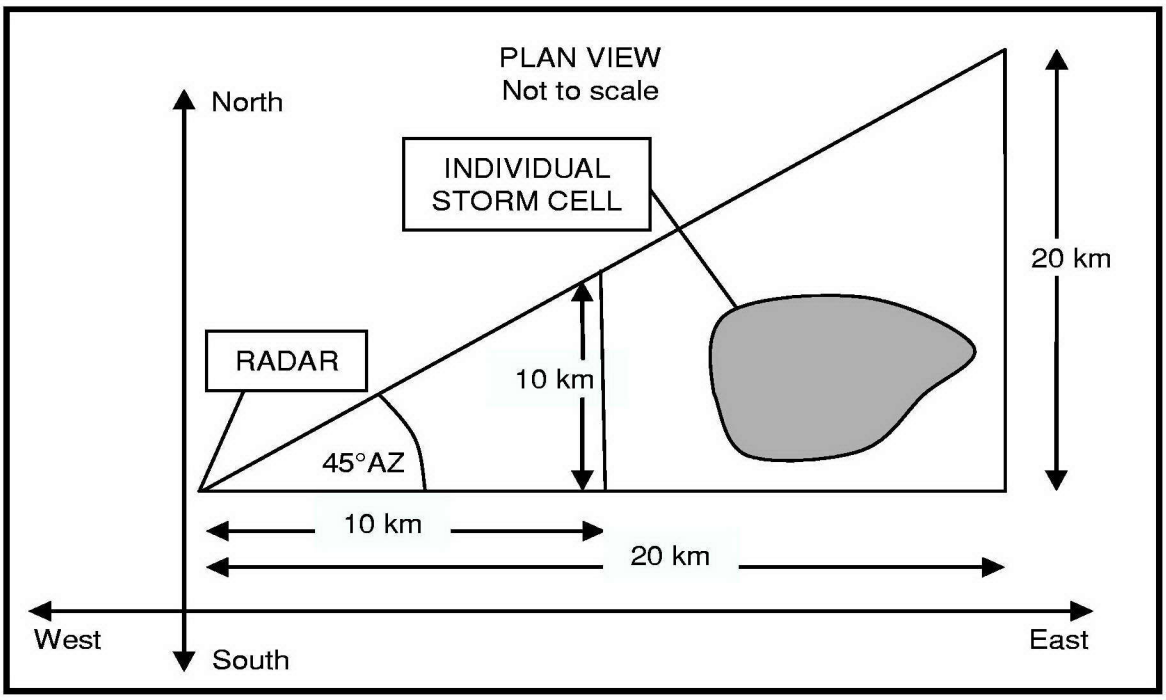

Figure 4.4. Radar 45° mechanical arc scan for multicellular storms.

C. ACCURACY OF MOMENT ESTIMATES

For meteorological measurements with the MWR-05XP, the desired nominal accuracies are ±1 dBZ for reflectivity measurements and ±1 m/s for Doppler velocity and spectrum width. Since the uncertainty associated with a single sample of return power, velocity, or spectrum width is very large, the number of samples, M, must be increased. Increasing the number of samples from each beam position, however, increases the acquisition time per position reducing the overall volumetric update rate. The key is to find a balance between accuracy and sample time. For research applications, the accuracy of the moment estimates is fundamental. The number of samples required to achieve the desired accuracy will be determined then sampling strategies will be developed based on these values. The sampling approach utilized in this work is designed to produce independent samples. Hereafter, it is implied that samples means independent samples.

To minimize the scanning time for volumetric updates, Doppler and reflectivity samples for estimation are obtained simultaneously. That is, for the proposed scanning

strategies, separate scans are not conducted for reflectivity and Doppler moment estimates. This will be explained in the section on development of sampling schemes. Pulse pair Doppler processing generally requires more samples than reflectivity processing for accuracy estimates of ±1 m/s and ±1 dBZ. For this reason, the more stringent Doppler sampling requirements will be developed first. The number of calculated Doppler samples is used to insure the ±1 dBZ reflectivity accuracy is met.

Recall that equation (3.64) gives the variance, $\mathrm{var}(\hat{v})$, for mean Doppler velocity. Rearranging (3.64) to solve for the number of samples in terms of the required variance gives:

$$M \approx \frac{\sigma_v \lambda}{8\left(\mathrm{var}(\hat{v})\right) T_s \sqrt{\pi}}. \tag{4.1}$$

where, σ_v = signal spectrum width, λ = radar wavelength, M = number of samples, and T_s = sample time. For a Doppler accuracy of ±1 m/s ($\mathrm{var}(\hat{v})$ of 1 m^2/s^2) with σ_v = 2.0 m/s (tornadic measurements), λ = 0.032 m, and T_s = 0.0001 s, the number of samples required is 45. For σ_v = 4.0 m/s (severe storm measurements), 90 samples are required for the same accuracy.

Equation (3.68) gives the spectrum width variance, $\mathrm{var}(\hat{\sigma}_v)$. Rearranging (3.68) for the number of samples in terms of the required variance gives:

$$M \approx \left(\frac{3\lambda^2}{128\sqrt{\pi}\left(\mathrm{var}(\hat{\sigma}_v)\right) T_s^2} \right) \sigma_{vn} \tag{4.2}$$

where, σ_{vn} is the rms spectrum width normalized by the unambiguous velocity interval,

$$\sigma_{vn} = \frac{2\sigma_v T_s}{\lambda}. \tag{4.3}$$

For a spectrum width accuracy of ±1 m/s with σ_v = 2.0 m/s (tornadic measurements), λ = 0.32 m, and T_s = 0.0001 s, the number of samples required is 17. For σ_v = 4.0 m/s (severe storm measurements), 34 samples are required for the same accuracy.

For the stated accuracies, the most stringent Doppler sample requirement was determined to be 45 for tornadic measurements, and 90 for severe thunderstorm clusters. In Figure 3.6, Marshall and Hitschfield (1953) show that 30 samples equate to the 80% confidence limits, 0.75 $\overline{P}$ and 1.25 $\overline{P}$. These limits correspond to + 1 dB and -1.3 dB. According to Figure 3.6, increasing the number of samples to 45 or 90 insures reflectivity accuracy well within the required ±1 dB. With the required accuracies met, sampling schemes based on 45 and 90 samples respectively for tornadic and severe storm clusters are presented below.

D. DEVELOPMENT OF SAMPLING SCHEMES

1. General Considerations

Smaller spectrum width increases the decorrelation time τ_i (ref. Figure 3.8). For reflectivity measurements, this means, that for a given frequency, it takes longer to obtain uncorrelated samples thus increasing the overall volumetric scan time. To overcome this limitation, the transmitted frequency must be varied for subsequent samples by at least $1/\tau$, where τ = the radar pulse width. This is because the transmitted pulse at frequency f has its energy concentrated in the band τ^{-1} centered on f. Therefore, uncorrelated weather signals are obtained by shifting the frequency by more than τ^{-1} in successively transmitted pulses (Doviak and Zrnic 1993).

For the MWR-05XP (τ = 1 μs), a shift of 1 MHz for successive pulses assures uncorrelated weather samples. A shift in transmitted frequency also results in a consequent steering of the radar beam (ref. Ch II). The resultant radar beam steering varies between 0.010° and 0.015° per 1 MHz depending on the elevation. This is approximately an order of magnitude less than the beam pointing resolution accuracy of 0.2° Az and El which means that a 1 MHz frequency shift essentially illuminates the same resolution volume. Currently, the MWR-05XP utilizes 20 MHz steps for frequency shifting. An average shift of 0.25° per 20 MHz is used in sampling scheme development. This beam shift must be accounted for and can be accomplished by incorporating a

frequency shift pointing correction (see recommendations, Ch VI) when a series of frequency shifted pulses collectively results in beam steering greater than the 0.2° pointing resolution accuracy.

For Doppler measurements, smaller spectrum width increases the maximum sample time, T_s, for correlated samples. While this does not directly facilitate a reduction in the overall volumetric scan time, it does, in general, add diversity to the sampling scheme by relaxing the successive pulse sampling requirement for correlated weather signals. Doppler estimates are obtained from pairs of pulses transmitted at the same frequency. Pulse pair processing, from the argument of the complex covariance (ref. Ch III) is computed from equation (3.62) for a single pair of correlated pulses and from equation (3.63) for N pairs of correlated pulses.

Doppler and reflectivity samples for estimation are obtained simultaneously. For the MWR-05XP, the sampling process adheres to the following format. Pairs of correlated pulses are Doppler processed with each subsequently transmitted pulse pair incrementing in 20 MHz steps. Reflectivity processing ignores the second pulse in each pulse pair and integrates only the first pulse of subsequently transmitted 20 MHz incremented pulse pairs.

Figure 4.5 illustrates the 94 μs phase shifter settling time when electronically steering the beam with the phase shifters. This means that any change in beam steering elevation adds a 94 μs delay. Frequency shifting in 20 MHz steps is accomplished between pulse pairs and adds a 50 μs delay for oscillator settling time. When simultaneously steering the beam in elevation and shifting the frequency, the 94 μs phase shift delay allows for the frequency oscillator to settle (50 μs) before transmitting the next pulse pair. Hence, it is advantageous to incorporate frequency shifting simultaneously with phase shifting when possible. The frequency agility of the radar significantly reduces the volumetric sampling time and facilitates versatility in scanning schemes.

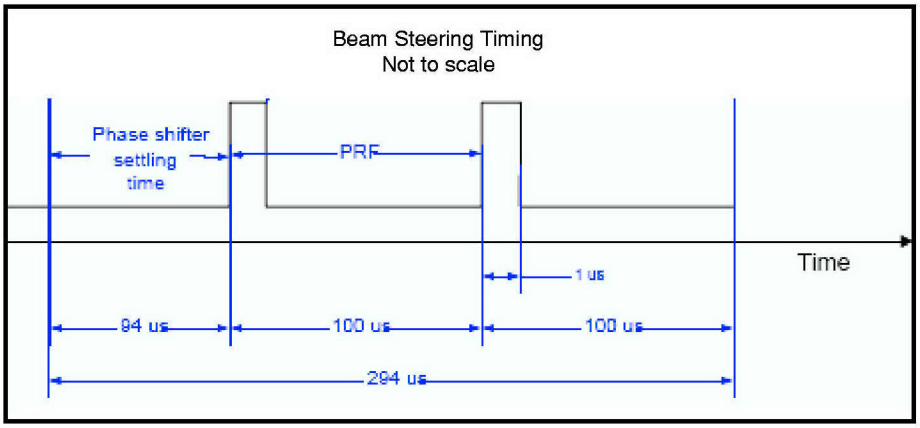

Figure 4.5. MWR-05XP beam steering (After PopStefanija 28 Oct, 2004).

To increase the sample rate, a PRF of 10 KHz is utilized in the sampling schemes for both tornadic and severe storm clusters. This limits the unambiguous range, Equation (3.6), to 15 km and unambiguous velocity, equation (3.8), to 75 m/s. Aliased range and velocity data are not addressed in this research but the WRP utilizes algorithms for aliased data.

2. Isolated Tornadic Storms

The sampling scheme for tornadic storms is shown in Figure 4.6 and is an adaptation of the raster scan in Figure 2.12a. This figure is a side view from the radar's perspective illustrating the beam positions, B_n 1-1 to 11-4 for the spatial sampling scales in Figures 4.1 and 4.2. In Figure 4.6, B_n 1-1 across (in azimuth) to B_n 1-4 represents approximately four 1.8° beamwidths or roughly 600 m azimuth at a distance of 5 km from the radar. B_n 1-1 up in elevation to 11-1 represents eleven 2.0° beamwidths or roughly 2 km El at a distance of 5 km. For this sampling scheme, the radar antenna is stationary which eliminates Doppler spectrum width contamination, equation (3.47), due to beam smearing. Azimuth and elevation scanning are accomplished by frequency steering and phase shifting respectively.

The sampling scheme proceeds as follows: a) starting at B_n 1-1, 3 pulse pair samples are frequency shift acquired at 9.37, 9.39, and 9.41 GHz, b) the beam is frequency steered to 9.51 GHz to acquire 3 samples from B_n 1-2 by frequency shifting from 9.51 to 9.53 to 9.55 GHz, c) the process is repeated for B_n 1-3 (9.65 – 9.69 GHz) and B_n 1-4 (9.79 – 9.83 GHz), d) the beam is electronically steered in elevation (phase

shifting) and frequency steered in azimuth to B_n 2-1 where the process repeats again starting at 9.37 GHz. This process completes a volume scan from B_n 1-1 to B_n 11-4 consisting of 3 samples of each beam position. 45 samples are needed to insure the required accuracy of ±1 m/s velocity and ±1 m/s spectrum width is met and, for reflectivity, within ±1 dBZ. The volume (B_n 1-1 to B_n 11-4) is scanned 14 more times to acquire 45 samples. As shown in Figure 4.6, 33.484 ms is needed for 3 samples of the volume (B_n 1-1 to B_n 11-4), therefore, 502.26 ms is required for a complete volume scan of 45 samples.

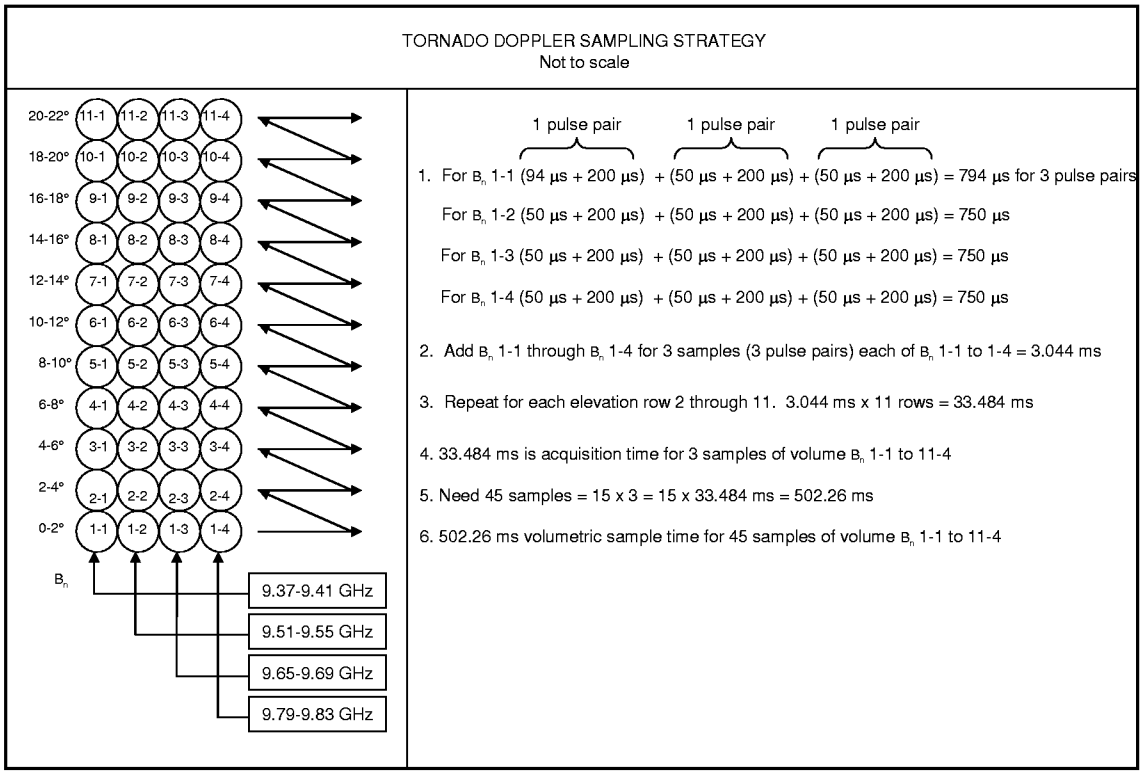

Figure 4.6. Proposed tornado Doppler sampling strategy.

3. Multicellular Severe Storm Clusters

The sampling scheme for multicellular severe storm clusters is shown in Figure 4.7 and is a combination of the raster and fixed frequency elevation scans in Figure 2.12. Figure 4.7, like 4.6, is a side view from the radar's perspective illustrating the beam positions, B_n 1-1 to 11-25 for the spatial sampling scales in Figures 4.3 and 4.4. In Figure 4.7, B_n 1-1 up to B_n 11-1 represents eleven 2.0° beamwidths or roughly 10 km El at a distance of 20 km from the radar. B_n 1-1 across to B_n 1-25 represents 25 1.8°

beamwidths or roughly 20 km Az at a distance of 20 km. For this sampling scheme, the antenna is sector scanned 45° in 4 seconds or 11.25°/second. Azimuth scanning is accomplished by antenna rotation and elevation scanning is controlled by phase shifting. The antenna scans left to right (clockwise viewed from above) for the lower 22° as shown in Figure 4.7, then mechanically elevates and scans back from right to left for the upper 22°. The rational for frequency backscanning will be discussed after the sampling scheme procedure is covered.

Severe storm clusters require 90 samples to achieve Doppler velocities accurate to ±1 m/s. The following scanning strategy utilizes 45 samples per beam position to meet the stated volumetric update requirement of 10 seconds. Adjacent range bin averaging is utilized to double the number of samples to 90 to meet the ±1 m/s Doppler accuracy. For the MWR-05XP the pulse volume (range bin) is 1.8° x 2.0° x 150 m. Doubling the pulse volume length (in range time) provides the necessary number of samples but reduces the range resolution to 1.8° x 2.0° x 300 m. The reduced accuracy is a reasonable tradeoff in order to minimize the volumetric sampling time.

The clockwise sampling scheme (ref. Figure 4.7) proceeds as follows: a) starting at B_n 1-1, 3 pulse pair samples are frequency shift acquired at 9.50, 9.52, and 9.54 GHz, b) the beam is electronically steered in elevation (phase shifting) to B_n 2-1 and the scan is repeated three times (at 9.50, 9.52, and 9.54 GHz) at each beam position for B_n 2-1 up to B_n 11-1, c) the beam is phase shifted back down and frequency backscanned to B_n 1-1 then scanned up the column three more times to B_n 11-1 at 9.48, 9.50, and 9.52 GHz, d) the B_n 1-1 to B_n 11-1 column is scanned an additional 9 times (3 times each at the next lower consecutive F_b frequency) to acquire a total of 45 samples for each beam position in the column (3 samples x 15 total scans), e) the 15 scans take 131.01 ms so a delay of 28.99 ms is required to allow the antenna to rotate to the next column position, B_n 1-2, f) the process (steps a through e) is repeated up each column from B_n 1-2 to B_n 1-25. The total time for 45 samples of the volume, B_n 1-1 to B_n 11-25, is 4 seconds (limited by antenna rotation rate of 11.25°/sec). Assuming 1 second to mechanically elevate the antenna up 22° and 4 seconds to repeat the scanning process from right to left, a volumetric update of approximately 10 seconds for 45° Az x 46° El scan is reasonable.

The antenna rotation at a rate of 11.25°/sec results in ≈ 1.47° of rotation during the 131.01 ms to acquire 45 samples from every beam position in each column. Frequency backscanning, F_b, is utilized to reduce this effect, referred to as beam smearing, by shifting the beam back in the opposite direction of antenna travel. This insures all samples from each beam position occupy essentially the same volume in space. An average value of 0.25°/20 MHz is used for F_b calculations. As shown in Figure 4.7, a F_b scheme of one 20 MHz step, a 40 MHz step, followed by two 20 MHz steps is applied after 3 consecutive column scans. That is, 3 column scans are accomplished at 9.50-9.54 GHz, the next three scans are accomplished at a F_b of 20 MHz lower (9.48-9.52 GHz), three more scans at a F_b of 40 MHz (9.44-9.48 GHz), another three scans at a F_b of 20 MHz (9.42-9.46 GHz), and the last three scans at a F_b of 20 MHz (9.40-9.44 GHz). Every 3 column scans takes 26.202 ms during which the antenna rotates ≈ 0.295°. Each 20 MHz of F_b repositions the beam back an average of 0.25° opposite to antenna travel. Net beam position change in azimuth for a complete set of 15 column scans is forward antenna rotation (0.295° x 5) minus F_b correction (0.25° x 3 + 0.50°) = 0.225°. From Keeler and Frush (1983) the antenna scan induced spectral width in m/s is given by

$$\sigma_{scan} = 0.2\omega D, \tag{4.4}$$

where ω = scan rate in rad/sec, D = antenna diameter in meters. For this scanning strategy, the MWR-05XP corrected antenna rotation rate is 0.03 rad/sec. This gives an approximate scan induced spectral width of 0.007 m/s, essentially eliminating this bias from the Doppler spectrum width equation (3.47).

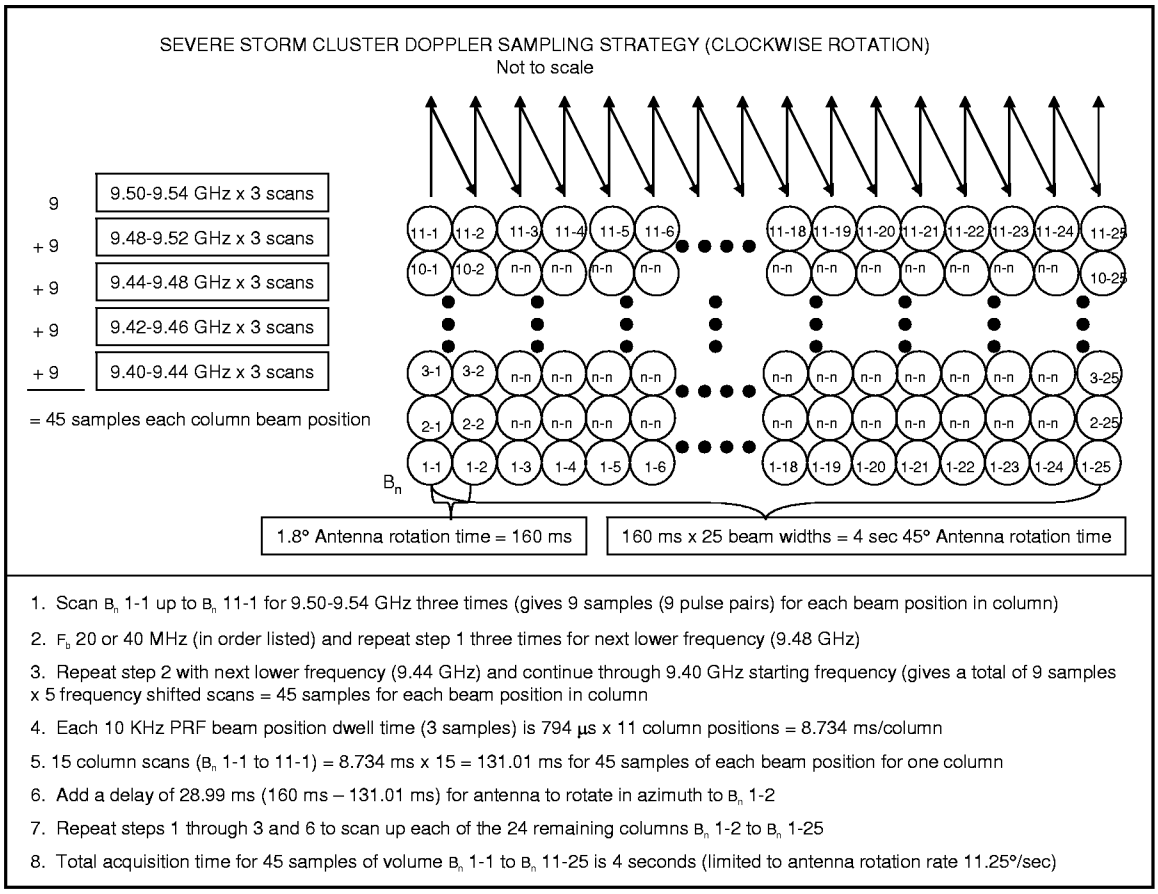

Figure 4.7. Proposed severe storm cluster Doppler sampling strategy.

V. PROPOSED SCANNING STRATEGY FOR OPERATIONAL APPLICATIONS

For operational applications, the sampling strategy and number of samples is determined by assumptions about the MWR-05XP operating parameters. These assumptions determine what compromises in accuracy and coverage are necessary to insure timely meteorological updates with minimum impact to normal radar search and track functions. The accuracies of the parameter estimates are then determined based on the number of samples and the sampling scheme. Spectrum width data is not considered for the operational scanning strategy. For clarity, the terms radar and MWR-05XP are used interchangeably in this chapter.

A. ASSUMPTIONS AND COMPROMISES FOR OPERATIONAL WEATHER SCANNING

Operational weather scanning must be able to detect a wide variety of meteorological phenomena. In general, the operational goal is to measure reflectivity and velocity with a volumetric update on the order of a few minutes. Assumptions about weather phenomena and the radar are: 1) spectrum width values of ≤ 8 m/s for 90% of any given storm volume (Doviak and Zrnic 1993), 2) antenna completes full 360° rotations at 3 rpm (18°/sec), 3) the WRP controls the antenna and all aspects of transmission and processing for the duration of the weather scan, 4) weather scan provides both reflectivity and velocity data and covers the maximum radar range (75 km), and 5) a full volumetric scan update on the order of a few minutes.

In an operational setting, the radar location is determined solely from its primary mission as a search and track radar. Figure 5.1 illustrates the proposed radar scan geometry. This geometry is a compromise that allows the radar to: 1) complete a full volumetric scan in 4 antenna revolutions, 2) capture the height scale (10 km) of convective storms, and 3) provide both reflectivity and limited velocity information simultaneously. The figure shows two antenna elevations. The antenna completes two azimuth revolutions at the lower elevation consisting of six electronic elevation scans covering 0° to 12°. Next, the antenna is mechanically elevated to 12° and completes an

additional two revolutions electronically scanning selected elevations between 12° and 34°. The highest scan at 34° limits the radar coverage to approximately 13 km.

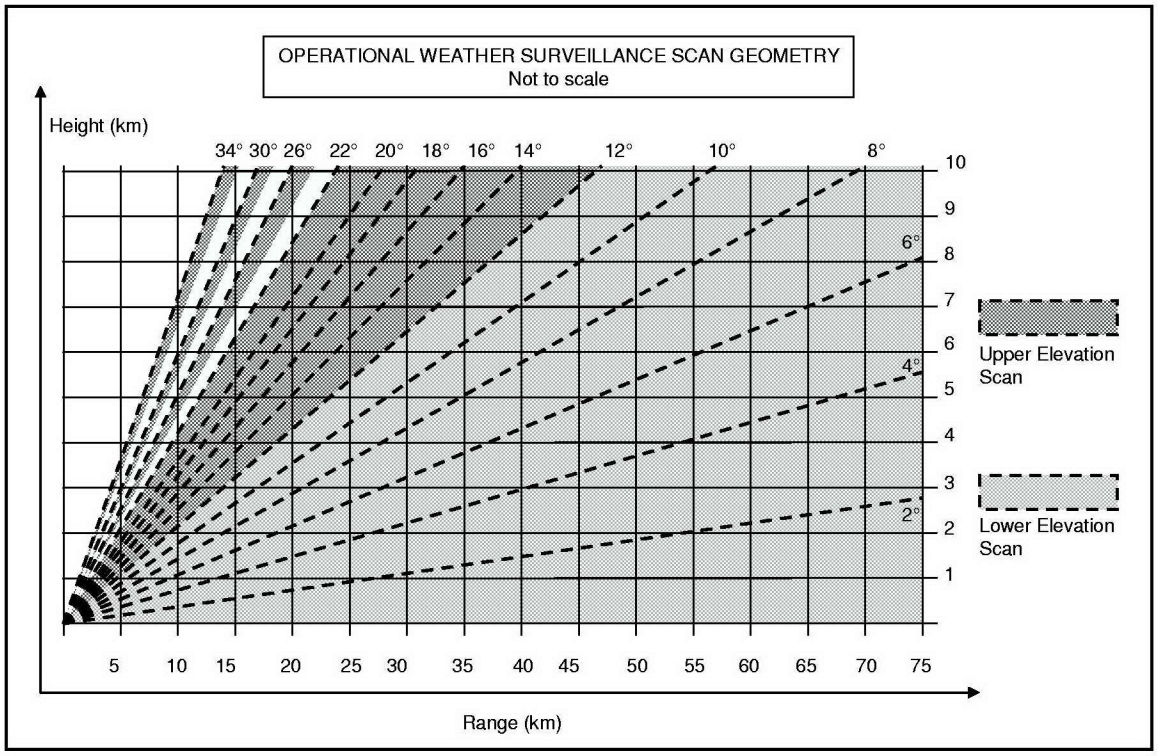

Figure 5.1. MWR-05XP operational radar scan geometry.

A limit of 4 antenna rotations at 3 rpm coupled with the 75 km range drive the following compromises: 1) reflectivity and velocity coverage is between 13 km and 75 km, 2) unambiguous velocity is 32 m/s from 13 - 37 km and 16 m/s from 37 - 75 km, 3) a volumetric update on the order of 80 seconds, and 4) a no data gap of approximately 18° Az during the antenna mechanical elevation time. The rationale for these compromises is addressed in the sampling scheme section below. The MWR-05XP coverage area for operational weather scanning is shown in Figure 5.2. Note that the first compromise defines an area without coverage or "cone of silence" within 13 km of the radar.

As done with research applications, Doppler and reflectivity samples for estimation are obtained simultaneously and the sampling process adheres to the following format. Pairs of correlated pulses are Doppler processed with each subsequently

transmitted pulse pair incrementing in 20 MHz steps. Reflectivity processing ignores the second pulse in each pulse pair and uses only the first pulse in each stepped frequency pair.

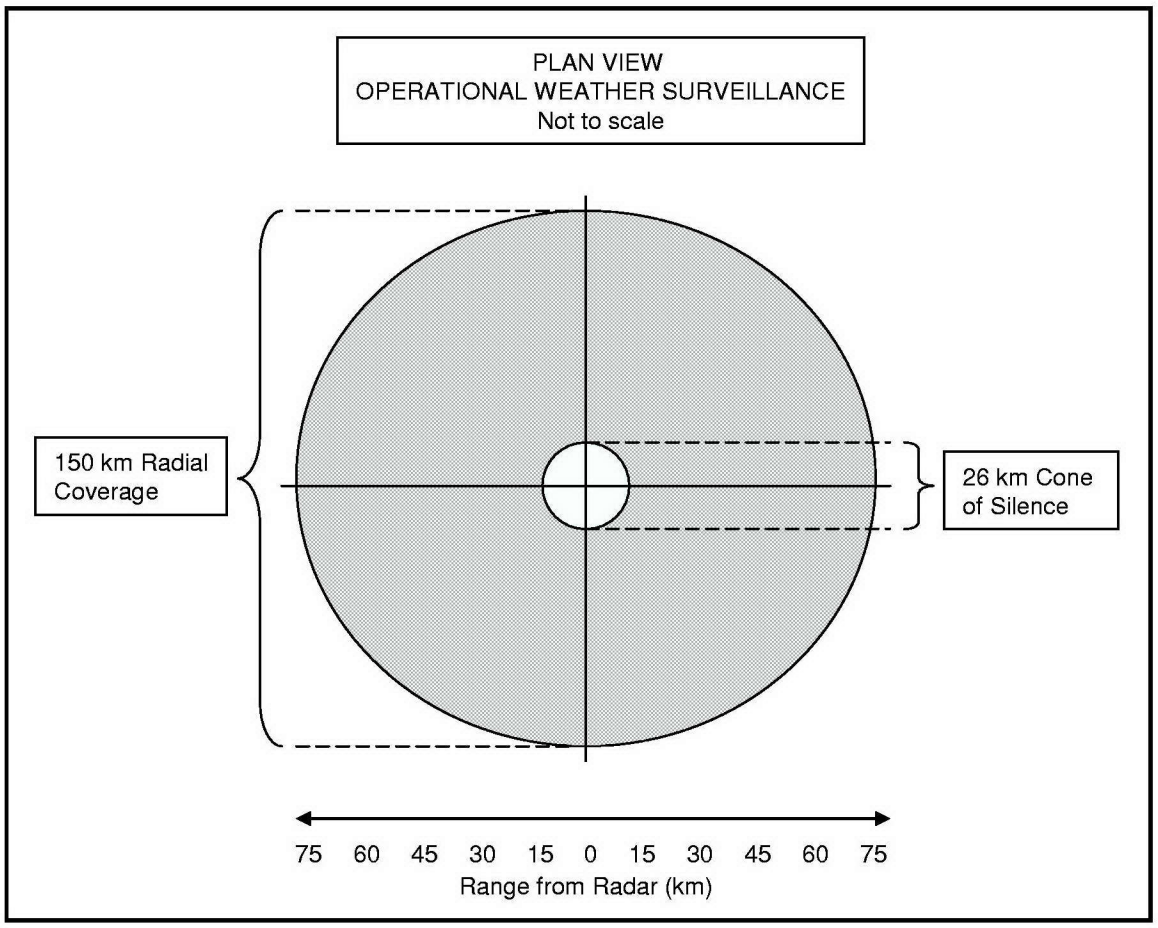

Figure 5.2. MWR-05XP operational weather scan coverage.

B. SAMPLING SCHEME FOR OPERATIONAL WEATHER SCANNING

The sampling scheme for operational weather scanning is shown in Figures 5.3 and 5.4. Figure 5.3 is a side view from the radar's perspective illustrating the lower elevation beam positions, B_n 1-1 to 6-200 for the scan geometry and coverage patterns in Figures 5.1 and 5.2. Each B_n in Figure 5.3 represents a 2.0° El x 1.8° Az beamwidth. For this sampling scheme, the antenna rotates 360° in 20 seconds or 18°/second and a 2 KHz PRF is used to prevent range aliasing. Azimuth scanning is accomplished by antenna rotation and elevation scanning is controlled by phase shifting. The antenna

completes two revolutions for the lower 12° as shown in Figure 5.3, then mechanically elevates to 12° and completes two more revolutions covering selected elevations between 12° and 34° as shown in Figure 5.4.

The lower elevation sampling scheme (ref. Figure 5.3) proceeds as follows: 1) starting at B_n 1-1, 3 pulse pair samples are frequency shift acquired at 9.50, 9.52, and 9.54 GHz, 2) the beam is electronically steered in elevation (phase shifting) to B_n 2-1 and the scan is repeated three times (at 9.50, 9.52, and 9.54 GHz) at each beam position for B_n 2-1 up to B_n 6-1, 3) the B_n 1-1 to B_n 6-1 column is scanned an additional 4 times (one time each at the next lower consecutive F_b frequency) to acquire a total of 15 samples for each beam position in the column (3 samples x 5 total scans), 4) the 5 scans take 95.82 ms so a delay of 4.18 ms is required to allow the antenna to rotate to the next column position, B_n 1-2, 5) the process (steps 1 through 4) is repeated up each column from B_n 1-2 to B_n 1-200. The total time for 15 samples of the volume, B_n 1-1 to B_n 11-200, is 20 seconds (limited by antenna rotation rate of 18°/sec). A full 360° Az x 12° El scan gives a volumetric update rate on the order of 20 seconds. The lower elevation scan is repeated for a total of 30 samples in 40 seconds.

The antenna rotation at a rate of 18°/sec results in ≈ 1.72° of rotation during the 95.82 ms to acquire 15 samples from every beam position in each column. As with research applications, frequency backscanning is utilized to reduce the beam smearing. An average value of 0.25°/20 MHz is used for F_b calculations. As shown in Figure 5.3, a F_b scheme of one 40 MHz step, a 20 MHz step, another 40 MHz step, and a 20 MHz step is applied after each column scan. That is, a column scan is accomplished at 9.50-9.54 GHz, the next scan at a F_b of 40 MHz lower (9.46-9.50 GHz), the next at a F_b of 20 MHz (9.44-9.48 GHz), the next at a F_b of 40 MHz (9.40-9.44 GHz), and the last scan at a F_b of 20 MHz (9.38-9.42 GHz). Every column scan takes 19.164 ms during which the antenna rotates ≈ 0.344°. Each 20 MHz of F_b repositions the beam back an average of 0.25° opposite to antenna travel. Net beam position change in azimuth for a complete set of 5 column scans is forward antenna rotation (0.344° x 5) minus F_b correction (0.25° x 2 + 0.50° x 2) = 0.22°.

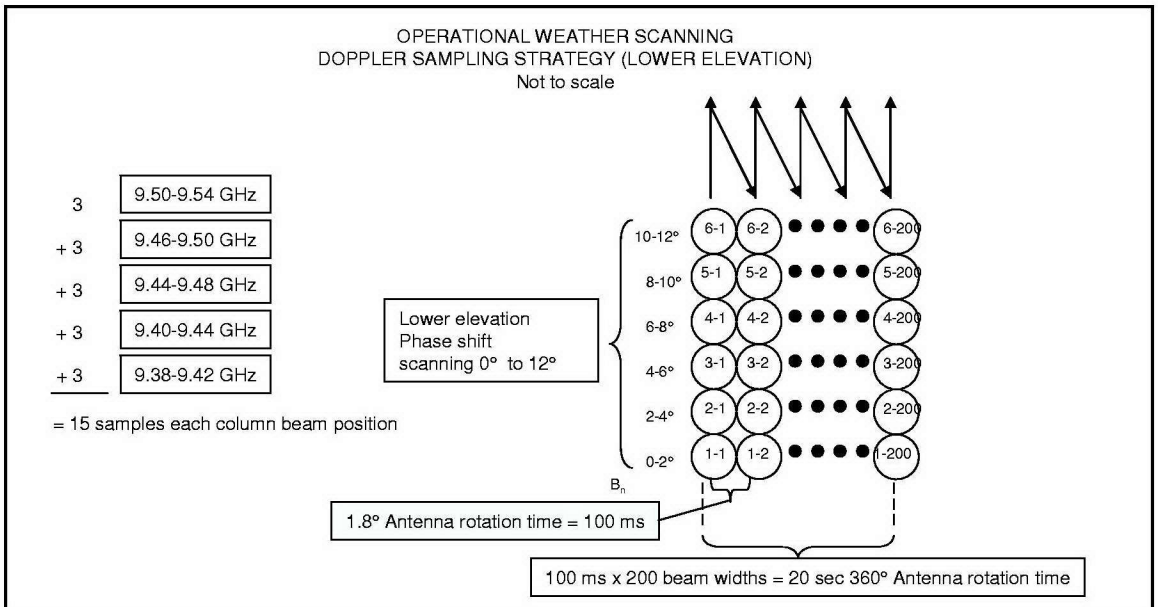

1. Scan B_n 1-1 up to B_n 6-1 for 9.50-9.54 GHz (gives 3 samples (3 pulse pairs) for each beam position in column)
2. F_b 20 or 40 MHz (in order listed) and repeat step 1 for next lower frequency (9.46 GHz)
3. Repeat step 2 with next lower frequency (9.44 GHz) and continue through 9.38 GHz starting frequency (gives a total of 3 samples x 5 frequency shifted scans = 15 samples for each beam position in column
4. Each 2 KHz PRF beam position dwell time (3 samples) is 3.194 ms x 6 column positions = 19.164 ms/column
5. 5 column scans (B_n 1-1 to 6-1) = 19.164 ms x 5 = 95.82 ms time for 15 samples of each beam position for one column
6. Add a delay of 4.18 ms (100 ms – 95.82 ms) for antenna to rotate in azimuth to B_n 1-2
7. Repeat steps 1 through 3 and 6 to scan up each of the 199 remaining columns B_n 1-2 to B_n 1-200 (gives one 360° rotation of 15 samples in each beam position)
8. Repeat for a second 360° rotation for a total of 30 samples
9. Total acquisition time for 30 samples (2 rotations) of volume B_n 1-1 to B_n 6-200 is 40 seconds (limited to antenna rotation rate 18°/sec)

Figure 5.3. Proposed operational weather scan sampling strategy (lower elevation).

Figure 5.4 is the same as Figure 5.3 except it illustrates the upper elevation beam positions, B_n 7-1 to 14-200 for the scan geometry and coverage patterns in Figures 5.1 and 5.2. The upper elevation sampling scheme (ref. Figure 5.4) is identical to the lower scheme except there are 8 beam positions in each column and a 4 KHz PRF is used to increase the unambiguous velocity to 32 m/s within 37 km of the radar. The only differences in the upper elevation scheme relate to the frequency backscanning corrections for antenna motion.

For the upper elevation scheme, antenna rotation at a rate of 18°/sec results in ≈ 1.22° of rotation during the 67.76 ms to acquire 15 samples from every beam position in each column. An average value of 0.25°/20 MHz is used for F_b calculations. As shown in Figure 5.4, a F_b of 20 MHz is applied after each column scan. Every column scan

takes 13.552 ms during which the antenna rotates ≈ 0.244°. Net beam position change in azimuth for a complete set of 5 column scans is forward antenna rotation (0.244° x 5) minus F_b correction (0.25° x 4) = 0.22°.

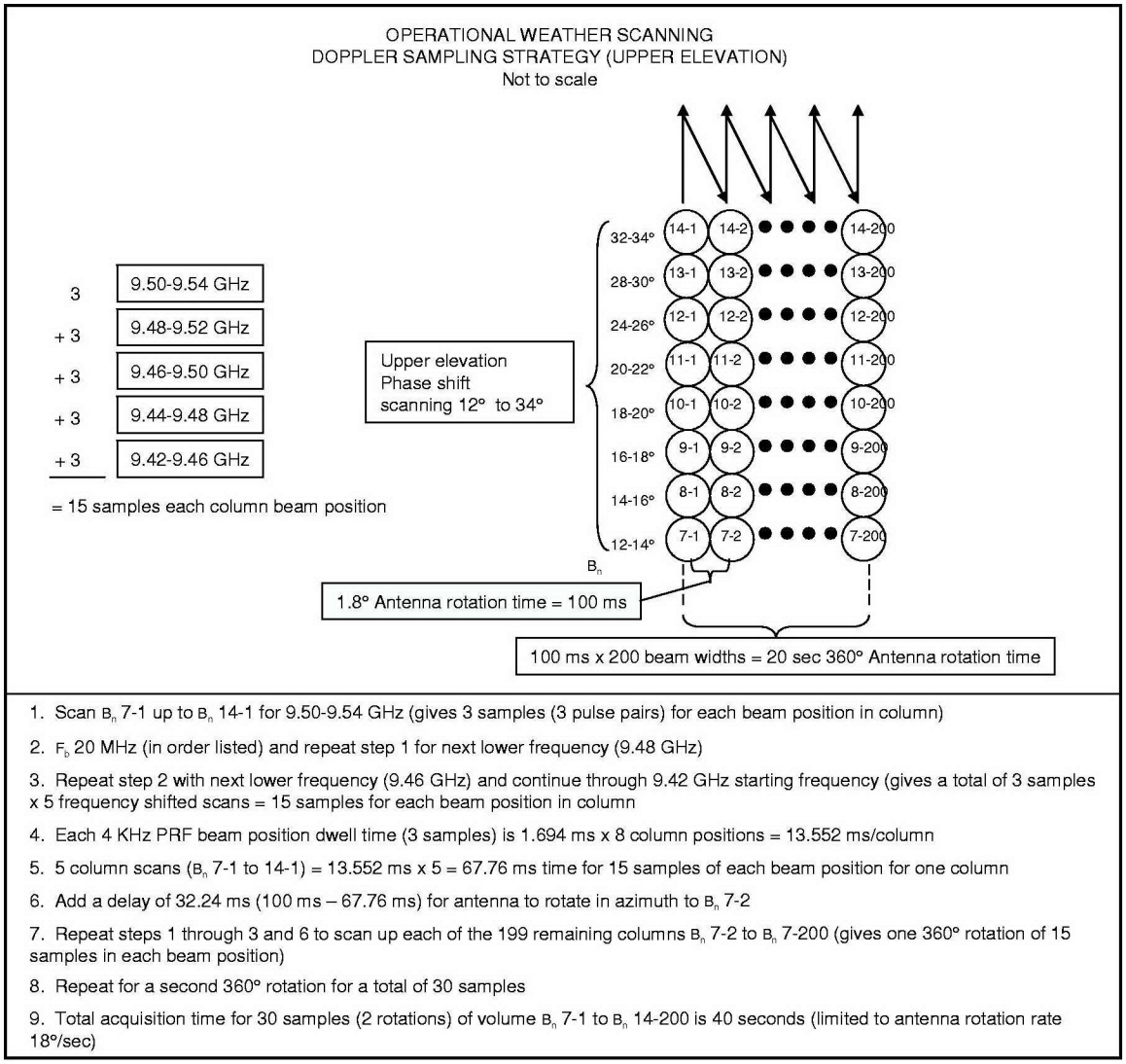

1. Scan B_n 7-1 up to B_n 14-1 for 9.50-9.54 GHz (gives 3 samples (3 pulse pairs) for each beam position in column)
2. F_b 20 MHz (in order listed) and repeat step 1 for next lower frequency (9.48 GHz)
3. Repeat step 2 with next lower frequency (9.46 GHz) and continue through 9.42 GHz starting frequency (gives a total of 3 samples x 5 frequency shifted scans = 15 samples for each beam position in column
4. Each 4 KHz PRF beam position dwell time (3 samples) is 1.694 ms x 8 column positions = 13.552 ms/column
5. 5 column scans (B_n 7-1 to 14-1) = 13.552 ms x 5 = 67.76 ms time for 15 samples of each beam position for one column
6. Add a delay of 32.24 ms (100 ms – 67.76 ms) for antenna to rotate in azimuth to B_n 7-2
7. Repeat steps 1 through 3 and 6 to scan up each of the 199 remaining columns B_n 7-2 to B_n 7-200 (gives one 360° rotation of 15 samples in each beam position)
8. Repeat for a second 360° rotation for a total of 30 samples
9. Total acquisition time for 30 samples (2 rotations) of volume B_n 7-1 to B_n 14-200 is 40 seconds (limited to antenna rotation rate 18°/sec)

Figure 5.4. Proposed operational weather scan sampling strategy (upper elevation).

During each of the 4 (2 lower and 2 upper elevation) antenna rotations, the received reflectivity and velocity information is stored in a buffer. After completion of the 4 rotations, the data (30 samples from each beam position) is integrated and output to display or storage as a volumetric update. Assuming 40 seconds for the lower elevations rotations, 1 second to mechanically elevate the antenna up to 12° and 40 seconds to

complete two rotations at the upper elevation, a volumetric update (minus the 18° Az no data gap in the upper elevation) of approximately 81 seconds for 360° Az x 34° El scan is reasonable.

C. ACCURACY OF MOMENT ESTIMATES

Only reflectivity and Doppler velocity accuracies will be addressed as spectrum width measurements would likely be of little value or be misinterpreted by the end-user. This is because end-users in an operational setting are primarily non-meteorological personnel. In an operational setting, fewer samples are taken to minimize the meteorological scan time and allow the radar to return to its primary search and track functions. Additionally, the basic antenna rotation rate and direction used to collect the weather samples is the same as normal radar search and track functions. This facilitates timely switching between meteorological and search and track scans reducing the impact to normal radar operations. Some accuracy, therefore, is sacrificed to accommodate these considerations.

Reflectivity for 30 samples is the same as stated in Ch III, ref. Figure 3.6. In the figure, Marshall and Hitschfield (1953) show that 30 samples equate to the 80% confidence limits, 0.75 $\overline{P}$ and 1.25 $\overline{P}$. These limits correspond to + 1 dB and - 1.3 dB. Defaulting to $\pm$ 1.3 dBZ still provides excellent accuracy for operational settings.

For σ_v = 8.0 m/s, λ = 0.031 m, and T_s = 0.0005 s (PRF 2 KHz), and 30 samples, and assuming large SNR, narrow spectrum widths, and contiguous pairs, equation (3.64) give the variance, $\mathrm{var}(\hat{v})$, for mean Doppler velocity as 1.17 m^2/s^2 or an accuracy of $\pm$ 1.08 m/s for the lower elevation volume scan. For the upper elevation volume scan with T_s = 0.00025 s (PRF 4 KHz), equation (3.64) give the variance, $\mathrm{var}(\hat{v})$, for mean Doppler velocity as 2.33 m^2/s^2 or an accuracy of $\pm$ 1.53 m/s. Accepting the lower $\pm$ 1.53 m/s accuracy for the entire volumetric scan still provides excellent accuracy for operational settings.

THIS PAGE INTENTIONALLY LEFT BLANK

VI. CONCLUSIONS AND RECOMMENDATIONS

A. CONCLUSIONS

This work is based on the limited availability of data and careful exclusion of classified information about the MWR-05XP. Scanning strategies for research and operational applications were developed for meteorological measurements with an experimental PAR, the MWR-05XP. Unique features of the MWR-05XP utilized to increase the scanning rate include frequency shift and frequency backscan along with phase shift scanning techniques. For research applications, the desired accuracies of the moment estimates were used to determine the number of samples required for two scanning strategies. The number of samples, along with the weather phenomena spectrum widths and sampling scales, were used to develop sampling strategies based on the known capabilities of the MWR-05XP. The desired accuracies for research applications were ±1 dBZ for reflectivity and ±1 m/s for Doppler velocity and spectrum width. For these accuracies, 45 and 90 samples were required for tornadic and severe thunderstorm clusters respectively. A tornadic storm sampling strategy was developed with a 7° Az x 22° El volumetric update of 502.26 ms and a volumetric resolution of 1.8° Az x 2° El x 150 m range. A sampling strategy for severe thunderstorm clusters was developed with a 45° Az x 46° El volumetric update of 10 seconds and a volumetric resolution of 1.8° Az x 2° El x 300 m range.

For operational weather scanning, the sampling strategy and number of samples were based on assumptions about the weather phenomena and the MWR-05XP operating parameters. These assumptions determined the compromises in accuracy and coverage to insure timely meteorological updates with minimum impact to normal radar search and track functions. The accuracies of the parameter estimates were then determined. A sampling strategy for operational weather scanning was developed with a 360° Az x 34° El volumetric update of 81 seconds and a volumetric resolution of 1.8° Az x 2° El x 150 m range. The resulting accuracies were ± 1.3 dBZ for reflectivity and ± 1.53 m/s for velocity.

This work has verified that, in general, for the acquisition of weather data, single frequency phased array radars offer only a slight sampling advantage over conventional scanning radars. This advantage is primarily from the time savings electronic beam steering (in elevation) offers over mechanical beam steering (in elevation). These savings are only on the order of one second per elevation scan. Factoring in the costs of phased array technology negates the modest gains in sampling rate. Obviously, a phased array antenna does not in itself facilitate dramatic improvements in the sampling rate. The fundamental sampling physics must still be satisfied. For example, there are over 5,000 2° beam positions in a hemisphere. For a 60 second scan, this provides only 6 ms dwell time for each beam position, which allows for only a few samples to make measurements. Reflectivity estimates, for example, require approximately 30 or more independent, uncorrelated samples for each beam position. A further constraint is that a decorrelation time on the order of 1 ms must elapse between consecutive samples in each beam position for the same frequency. In order to reduce the time to acquire samples, other methods, such as multiple beams or frequency diversity in addition to electronic beam steering, must be employed in combination. With appropriate antenna control and signal processing, phased array antennas can significantly increase the sampling rate through electronic beam steering, frequency diversity, or multiple beams.

This research verified that for meteorological sampling with the MWR-05XP, frequency diversity, coupled with electronic elevation scanning, offers a significant sampling advantage over conventional radars. The combination of electronic beam steering and frequency diversity produces a synergistic reduction in sampling time that increases the overall volumetric update rate. This synergy is realized primarily through enhanced sampling scheme diversity and, for research applications, a simple reduction in the sample space for specific phenomena.

This research has also shown that, based on assumptions about the MWR-05XP operating parameters, it is possible to incorporate operational weather scanning into the radar's multifunction capability. It is the author's opinion that future research and development should have a central goal to eventually incorporate WRPs into operational

AN/MPQ-64 radars and a capability to integrate operational meteorological data (OMD) from networked PARs into a common operating picture for battlefield commanders.

B. RECOMMENDATIONS FOR CONTINUED DEVELOPMENT

The following recommendations are priority ranked for continued development of the WRP-05XP as a research tool and eventual consideration to incorporate WRPs into existing tactical PARs. The recommended approach, therefore, is to develop this particular radar for research applications first and then focus on adapting and generalizing the WRP for use on currently fielded military PARs. It is assumed that basic functionality will be verified (according to the development contract) when the system is delivered at contract completion. Certainly, other issues and concerns about weather measurements for research and possible operational use will arise when the radar is delivered at contract completion.

Research development should initially focus on verification of basic functionality and measurement accuracy. Follow on work should concentrate on developing scanning strategies and algorithms for various atmospheric measurement applications where the radar's unique capabilities (beam steering and frequency agility) can be exploited. This is most likely in: a) the measurement of convective or other phenomena where the time scale of structural changes can not be resolved with currently fielded technology, and b) the measurement of near ground phenomena where the effects of ground clutter can be more effectively mitigated with the phased array antenna and signal processing.

The next major thrust should be to develop the WRP for use as an add-on capability to currently fielded PARs. Development should focus on simple reflectivity and Doppler velocity scanning strategies that can be incorporated into tactical PAR environmental sensing schemes. Finally, the capability to integrate this OMD from a system of networked PARs into a common operating picture (COP) for battlefield commanders should be pursued.

1. Calibration

Accurate measurement of received power requires that system losses and the input/output characteristics of the radar receiver be measured. The MWR-05XP antenna loss was measured and some calibration work has been attempted with the receiver.

During initial receiver calibration, the attenuator setting was not optimized, therefore, a higher saturation level is anticipated when the attenuator can be controlled with the WRP (Knorr 18 Feb, 2005). The receiver calibration, in Figure 6.1, shows a very linear input/output characteristic fit with a 3rd order polynomial curve. In the radar operational mode, minor variations in peak power and the interpulse period were observed on an oscilloscope. These must be deciphered before further receiver calibration can proceed (Knorr 8 Nov, 2004). Receiver calibration should be completed when the system is delivered at contract completion. An alternate method of calibration utilizing a standard radar sphere of known diameter should also be considered. Finally, comparison of simple reflectivity and Doppler products to another radar (i.e., a WSR-88D) should be conducted to verify basic functionality. Preliminary performance analysis (ref. Figure 2.8) suggest that input saturation at the receiver may occur for high reflectivity signals ($\geq$ 55 dBZ) within 10 km of the radar, therefore a programmable attenuator may be required at the receiver input.

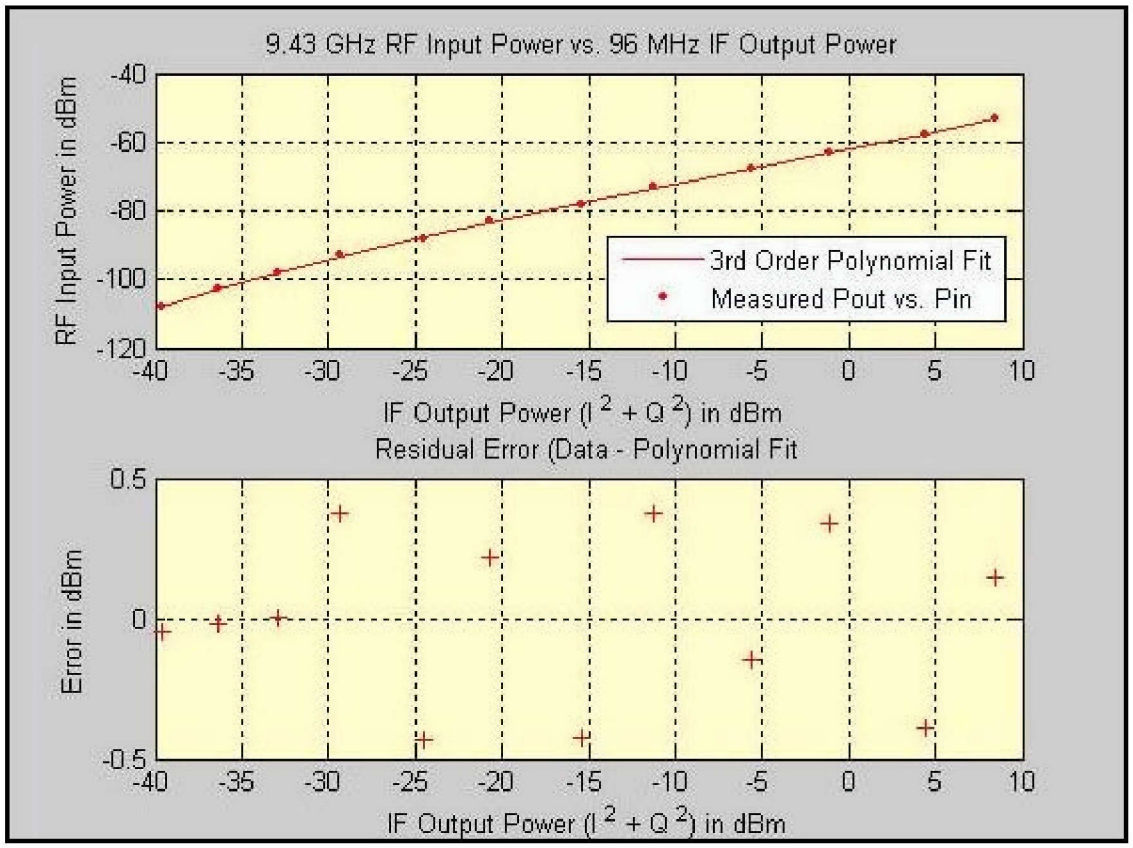

Figure 6.1. MWR-05XP preliminary receiver calibration.

2. Pointing Correction Algorithm.

For research applications utilizing frequency shift sampling schemes, a pointing correction algorithm must be incorporated for accurate placement of the sample volume in space. Frequency shift sampling steers the beam which collectively results in a slight non-linear shift of the true sample volume from the GPS positioned sample volume. Figure 6.2 illustrates this concept. This simple algorithm, which corrects each GPS indicted radar beam position to the actual sampled beam position, can be incorporated as a last step in the post processing section before the data is output. This is a fundamental concern if the radar is used for close range higher resolution data collection where the radar beamwidth can resolve features such as tornado funnel clouds or mesocyclones.

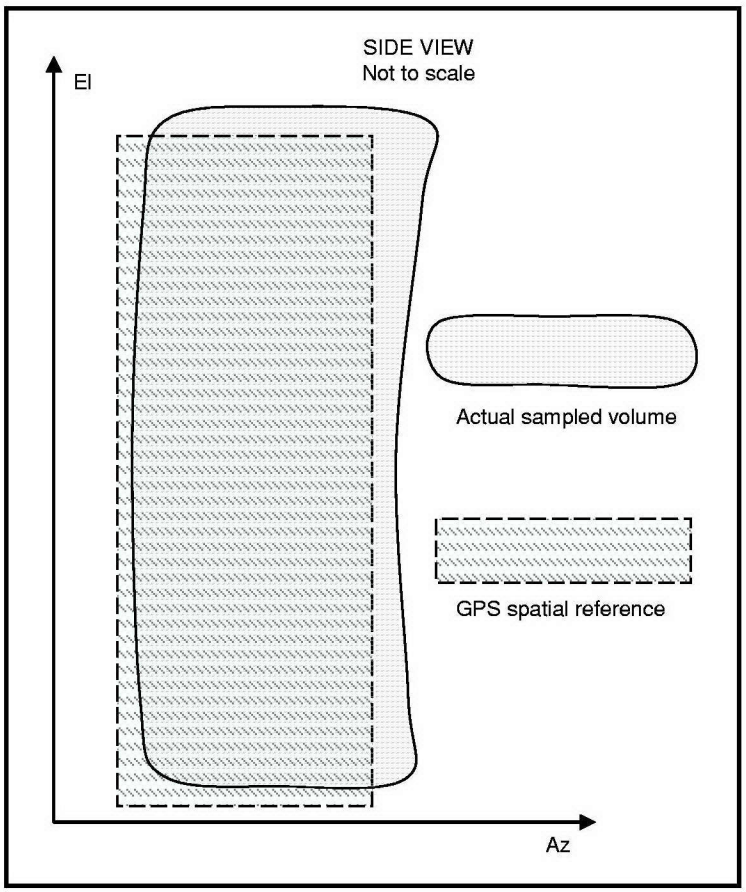

Figure 6.2. GPS indicated beam pointing versus actual beam pointing.

3. Verification of Velocity and Range Dealiasing Algorithms.

Mitigating the effects of ambiguities is necessary to obtain accurate and reliable data. The relatively short 3 cm wavelength and high PRFs utilized to increase the sampling rate fundamentally amplify range and velocity ambiguities. Existing WRP

dealiasing algorithms must be verified and optimized. The WRP dual and staggered PRTs must be incorporated into proposed scanning strategies to capitalize on the tremendous sampling advantages frequency diversity brings to phased array antennas. The WRP's FPGA controller and digital receiver/signal processor show promise to explore if phase coding and interlaced sampling techniques, discussed by Doviak and Zrnic (1993), can be incorporated into scanning strategies to address aliasing.

4. Modification for 1 MHz Frequency Scanning Increments.

A modification of the current 20 MHz frequency scanning step increment to 1 MHz should be investigated. This will require software and or hardware modification. A preliminary analysis of 1 MHz increment sampling for the proposed tornadic storm sampling scheme indicates a sample time reduction on the order of 16 ms. Simple extrapolation of these time savings to full hemispheric sampling reduces scanning time an additional 2 seconds. While these time reductions appear insignificant, higher resolution frequency scanning adds tremendous versatility to sampling scheme development by reducing undesired beam steering for consecutive independent pulses. Further investigation of the benefits that 1 MHz increment sampling can provide for the MWR-05XP is warranted.

5. Develop a Standard Suite of Output Products.

A suite of reflectivity, velocity, and spectrum width products along with 3-dimensional visualizations and 4-dimensional (time) algorithms should be developed. Many WSR-88D RHI and PPI products provide a benchmark for visualization and algorithm development efforts. In addition to base reflectivity, velocity, and spectrum width, WSR-88D products and algorithms (OFCM 1991) that show promise for application as MWR-05XP output products are listed in Table 6.1. To fully realize the rapid scan and volumetric update capability of the MWR-05XP, 4-dimensional algorithms that exploit the time domain should be explored. These 4-dimensional algorithms may be based on scan to scan changes in reflectivity, velocity, and spectrum width fields, and may provide fundamental insight into the time evolution of weather phenomena.

Combined Moment	Severe Weather Probability
Composite Reflectivity	Storm Relative Velocity
Cross Section	Storm Structure
Echo Tops	Storm Total Precipitation
Hail Index	Storm Track Information
Layer Composite Reflectivity	Storm Position Forecast
Mesocyclone	Tornadic Vortex Signature
Hourly Precipitation Accumulation	Velocity Azimuth Display (VAD)
Precipitation Rate	VAD Wind Profile
Severe Weather Analysis	Weak Echo Region

Table 6.1. WSR-88D products and algorithms for possible application as MWR-05XP output products.

6. Strategies for Improved Spectrum Width Measurements.

Scanning and processing strategies for improved spectrum width measurements should be developed. Beam steering with phased arrays (in elevation for the MWR-05XP) effectively reduces beam smearing to zero because the beam is essentially fixed in space during the data acquisition period. Frequency backscanning in azimuth can also effectively eliminate beam smearing. This improves spectrum width estimates by removing contamination due to antenna motion. Once reliable SW measurements can be made, adaptive scanning strategies should be pursued that take advantage of spectrum width measurements. These strategies can adapt in real time to optimize the dwell time, subject to a constraint on data quality, and hence, the sampling scheme for various weather phenomena (Doviak et. al 2001).

7. Strategies to Minimize Ground Clutter.

A method to adaptively train the antenna sidelobe pattern at each site for improved ground clutter suppression should be designed (Keeler and Frush 1983). Optimized ground clutter canceling and clutter suppression algorithms would allow true along the horizon scanning with sufficient ground clutter suppression for near surface measurements of reflectivity and Doppler velocity. Near surface reflectivity measurements would improve rainfall estimates and facilitate improved quantitative

precipitation algorithms. Doppler measurements near the surface would provide data for previously unobserved low-level mesocylonic rotations (Bluestein et. al 1993).

8. Operational Meteorological Scanning Strategies.

Develop reflectivity and Doppler velocity scanning schemes for operational use with fielded 3 and 5 cm PARs. This will likely evolve along one of two general lines. The first is that proposed meteorological scans may be incorporated into the normal scanning modes of the radar. The second is that meteorological scans may be taken while the PAR is in a maintenance type mode as proposed in this work. In this case, the WRP is controlling the radar while the radar is not performing its normal search and track functions. Although more complicated, the first approach, from a meteorological standpoint, is better because fully integrated meteorological scans would provide better time continuity for weather observations.

9. Integrate OMD into COP for Battlefield Commanders.

Develop a capability to integrate operational meteorological data from networked PARs into a common operating picture for battlefield commanders. The benefits of this data for command and control and operators are obvious. An awareness of impending hazardous weather would provide time for coordinated resource protection actions minimizing the impact to manpower and material. The availability of real-time radar information in hostile regions of sparse weather data would benefit both operations planning and mission execution. It is relatively easy to upchannel OMD, so the emphasis should be to develop the infrastructure to incorporate this information into a COP.

C. RECOMMENDATIONS FOR FUTURE STUDIES

1. Severe Storm and Tornado Measurements in Central US.

Two significant radar limitations in severe weather and type I (mesocyclone associated) tornado research are: a) the limited volumetric update capability (Wurman and Randall 2005), and b) the lower limit of near ground measurements due to ground clutter effects (Davies-Jones et. al 2001). The MWR-05XP, along with the Rapid-DOW radar, currently under development with the University of Oklahoma and the National Center for Atmospheric Research, can provide researchers the capability to interrogate these phenomena with significantly reduced scan times. In particular, near ground

Doppler measurements of low-level mesocyclogenesis may provide the connection between mid level and near ground rotation during tornado genesis. Understanding this connection is a key element to deciphering between mesocyclones that produce tornadoes and those that do not. The author's opinion is that the MWR-05XP is best suited to this type research and should be utilized primarily for convective research efforts.

2. Waterspout Measurements on Florida Coast.

The second fundamental type of tornado (type II) is not associated with a parent mesocyclone. These are generally small, short lived, weak tornadoes such as cold air funnels and waterspouts. The Florida coast and Keys provide both a spawning ground and excellent observation platform for waterspouts as coastal convergence zones provide low level support for their formation. Golden (1974) provides an excellent and in depth review of Florida Key waterspouts. The MWR-05XP is well suited to study these phenomena. Numerous cloud studies in this region of the US also provide opportunities for coordinated efforts between ground based radars and cloud penetration flights. The MWR-05XP has the capability and could be adapted to, according to Doviak et. al (2001), simultaneously track these aircraft while providing radar data for later comparison with the aircraft in-situ instrument data.

3. Stratiform and Convective Precipitation Measurements

A study comparing MWR-05XP rainfall measurements with networked rain gages should be conducted to develop and optimize quantitative precipitation algorithms for the radar. Once the precipitation algorithms have been developed, the MWR-05XP can be utilized as an adjunct to existing rain gage networks to facilitate precipitation studies. Current radar coverage along the western US coast, particularly coastal California, often significantly underestimates low-level stratiform rainfall amounts. Stratiform rain measurements along coastal topography with the MWR-05XP can provide increased coverage and improved rainfall estimates well below the lowest scan elevation of WSR-88D radars.

THIS PAGE INTENTIONALLY LEFT BLANK

LIST OF REFERENCES

Bluestein, H. B., J. G. LaDue, H. Stein, D. Speheger, and W. D. Unruh, 1993: Doppler radar wind spectra of supercell tornadoes. *Mon. Wea. Rev.,* 121, 2200-2221.

Davies-Jones, R., R. J. Trapp, and H. B. Bluestein, 2001: Tornadoes and tornadic storms. *Severe Convective Storms, Meteor. Monogr.*, No. 50, Amer. Meteor. Soc., 167-221.

Doswell, C. A., 2001: Severe convective storms-an overview. *Severe Convective Storms, Meteor. Monogr.*, No. 50, Amer. Meteor. Soc., 1-26.

Doviak, R. J., and D. S. Zrnic, 1993: *Doppler Radar and Weather Observations*, 2d ed. Academy Press, San Diego, 562 p.

_____, D. S. Zrnic, and A. Shapiro, 2001: Phased array weather radar-benefits and challenges. Preprints, *30th International Conf. on Radar Meteorology*, Munich, GE, Amer. Meteor. Soc., 202-204.

Fang, M., and R. J. Doviak, 2001: Relating WSR-88D spectrum width data to various weather conditions. Preprints, *30th International Conf. on Radar Meteorology*, Munich, GE, Amer. Meteor. Soc., 382-384.

Forsyth, D., NSSL, 2003: New radar technology can increase tornado warning lead times. [Available online at http://www.nssl.noaa.gov/par], February/2005.

Golden, J. H., 1974: Life cycle of florida keys' waterspouts. NOAA Tech. Memo ERL NSSL-70, 147p.

Johnson, K. W., 2000: Personal Communication, 4 Feb. MPQ-64, 1 pp. Raytheon Systems Company, Sensors and Electronic Systems Public Relations, PO Box 902, EO/E1/E107, El Segundo, CA 90245

Keeler, R. J., and C. L. Frush, 1983: Rapid scan doppler radar development considerations. Preprints, *21st Conf. on Radar Meteorology*, Alberta, Canada, Amer. Meteor. Soc., 284-290.

Kessler, E., 1983: *Thunderstorm Morphology and Dynamics*. Vol. 2, *Thunderstorms-A Social, Scientific, and Technological Documentary*, University of Oklahoma Press, 411 p.

Knorr, J. B., 2004: Personal Communication, 12 Oct. Sentinal performance charts, 5 pp. Naval Postgraduate School, Monterey, CA 93943

_____, 2004: Personal Communication, 8 Nov. MPQ-64 operational mode, 1 pp. Naval Post Graduate School, Monterey, CA 93943

_____, and D. C. Jenn, 2004: *Radar Meteorology, Handouts of the MR 3240 Course*. Naval Post Graduate School, Monterey, CA 93943

_____, 2005: Personal Communication, 28 Jan. MWR-05XP truck, 1 pp. Naval Post Graduate School, Monterey, CA 93943

_____, 2005: Personal Communication, 31 Jan. Ch 2 with new graph, 13 pp. Naval Post Graduate School, Monterey, CA 93943

_____, 2005: Personal Communication, 4 Feb. Truck drawings, 3 pp. Naval Post Graduate School, Monterey, CA 93943

_____, 2005: Personal Communication, 18 Feb. Radar cal curve, 1 pp. Naval Post Graduate School, Monterey, CA 93943

_____, 2005: Personal Communication, 16 Mar. MWR-05XP Pictures, 1 pp. Naval Post Graduate School, Monterey, CA 93943

Kraus, J. D., 1950: *Antennas*. McGraw-Hill Inc., New York, 553 pp.

Marshall, J. S., and W. Hitschfeld, 1953: Interpretation of the fluctucating echo from randomly distributed scatterers, Pt 1, *Can. J. Physics*., 31, 962-995.

NEXRAD Technical Requirements, 1991: Report # R400-SP401A, November. Copies available from the NEXRAD Joint System Program Office, Silver Spring, MD, 20910, 190 pp.

OFCM (Office of Federal Coordinator for Meteorological Services and Supporting Research), 1991: *Doppler radar meteorological observations, part C*. Federal Meteorological Handbook, No. 11. Copies available from OFCM, Rockville, MD, 20850.

PopStefanija, I., A. Pazmany, and R. Bluth, 2003: An X-band phased array doppler weather radar. Preprints, *31st Conf. on Radar Meteorology*, Seattle, WA, Amer. Meteor. Soc., 809-810.

_____, 2004: Personal Communication, 15 Oct. MPQ-64 Antenna, 8 pp. ProSensing Inc., 107 Amherst, MA 01002-1098.

_____, 2004: Personal Communication, 28 Oct. MPQ-64 Q & A, 2 pp. ProSensing Inc., 107 Amherst, MA 01002-1098.

_____, Prosensing, Inc., 2005: Add-on Weather Radar Processor for Tactical radar systems. [Available online at http://www.armyforum.com/virtual2004/briefings/Prosensing.pdf], January/2005.

Probert-Jones, J. R., 1962: The radar equation in meteorology. *Quart. J. Royal Meteor. Soc.*, 88, 485-495.

Raghaven, S., 2003: *Radar Meteorology*, Kluwer Academic Publishers, Netherlands, 549 p.

Sauvageot, H., 1992: *Radar Meteorology*, Artec House, Boston, 366 p.

Skolnik, M. L., 1990: *Radar Handbook*, 2d ed. McGraw-Hill Inc., New York.

Wurman, J. and M. Randall, University of Oklahoma/NCAR, 2005: An inexpensive, mobile, rapid-scan radar. [Available online at http://aaron.ou.edu/docs/radarconf-rapid-2001-0327.pdf], December/2004.

THIS PAGE INTENTIONALLY LEFT BLANK

INITIAL DISTRIBUTION LIST

1. Defense Technical Information Center
   Ft. Belvoir, Virginia

2. Dudley Knox Library
   Naval Postgraduate School
   Monterey, California

3. Dr. Carlyle Wash
   Department of Meteorology, Naval Postgraduate School (NPS)
   Monterey, California

4. Dr. Jeffrey Knorr
   Department of Electrical and Computer Engineering, NPS
   Monterey, California

5. Dr. Haflidi Jonsson
   Center for Interdisciplinary Remotely Piloted Aircraft Studies (CIRPAS)
   Monterey, California

6. Robert Bluth
   CIRPAS
   Monterey, California

7. Dr. Joshua Wurman
   School of Meteorology, University of Oklahoma
   Norman, Oklahoma

8. Dr. Howard Bluestein
   School of Meteorology, University of Oklahoma
   Norman, Oklahoma

9. Maj. Michael Miller
   Radar Operations Center, University of Oklahoma
   Norman, Oklahoma